ANALYSIS OF BODY AND TAIL OF A FLAPPING DRONE

CHAI YUAN

FACULTY OF ENGINEERING
UNIVERSITY OF MALAYA
KUALA LUMPUR

2020

ANALYSIS OF BODY AND TAIL OF A FLAPPING DRONE

CHAI YUAN

RESEARCH PROJECT SUBMITTED IN FULFILMENT OF THE REQUIREMENTS FOR THE DEGREE OF MASTER OF MECHANICAL ENGINEERING

FACULTY OF ENGINEERING
UNIVERSITY OF MALAYA
KUALA LUMPUR

2020

UNIVERSITY OF MALAYA

ORIGINAL LITERARY WORK DECLARATION

Name of Candidate: CHAI YUAN

Matric No: KQK190001

Name of Degree: Master of Mechanical Engineering

Title of Research Project: Analysis of body and tail of a flapping drone

Field of Study: Computer Fluid Dynamic Analysis

I do solemnly and sincerely declare that:

(1) I am the sole author/writer of this Work;
(2) This Work is original;
(3) Any use of any work in which copyright exists was done by way of fair dealing and for permitted purposes and any excerpt or extract from, or reference to or reproduction of any copyright work has been disclosed expressly and sufficiently and the title of the Work and its authorship have been acknowledged in this Work;
(4) I do not have any actual knowledge nor do I ought reasonably to know that the making of this work constitutes an infringement of any copyright work;
(5) I hereby assign all and every rights in the copyright to this Work to the University of Malaya ("UM"), who henceforth shall be owner of the copyright in this Work and that any reproduction or use in any form or by any means whatsoever is prohibited without the written consent of UM having been first had and obtained;
(6) I am fully aware that if in the course of making this Work I have infringed any copyright whether intentionally or otherwise, I may be subject to legal action or any other action as may be determined by UM.

Candidate's Signature Date:

Subscribed and solemnly declared before,

Witness's Signature Date:

Name:

Designation:

ANALYSIS OF BODY AND TAIL OF A FLAPPING DRONE

ABSTRACT

The Micro Aerial Vehicle (MAV) is a kind of unmanned aerial vehicle with a small size, which has a unique performance that larger aircrafts do not have. MAV can fly in confined spaces and perform hover, forward flight, etc. The flapping wing micro aerial vehicle is one type of flight imitates the insects (birds), which can fly based on the flapping wing. Compared with fixed-wing aircraft, the flapping wing micro aerial vehicle (FWMAV) has a smaller volume, lighter weight, and higher flight efficiency. FWMAV can be largely used in military and civil applications. In this project, the flapping drone is a type of flapping wing micro aerial vehicle. The aerodynamic focus of the fuselage will move behind the center of gravity due to the effect of the tail. At the same time, the different angles of the tail surface will produce different moments to change the flight attitude of flapping drone and maintain a corresponding balance. Based on the research about the flying mechanism of birds and insects, this research project presented some aspects: the control of flying attitude, the angle between tail and body, the model of body and tail. An improved flapping drone model was designed according to the prototype, which includes some main components: wing, tail, fuselage, control system, mechanical structure. The effects of the different angle of the tail were tested under different inlet velocity. Moreover, we considered different pitch angles (from -45°to +45°) of the fuselage to simulate the real flying attitude based on the ANSYS method and actual experiment. After compared different conditions, the reasonable 20° tail angle was chosen in this project.

Keywords: Flapping drone, CFD, Lift force, Tail, ANSYS

ANALISIS BADAN DAN EKOR KENDERAAN UDARA MIKRO FLAP

ABSTRAK

Kenderaan Udara Mikro (MAV) adalah sejenis kenderaan udara tanpa pemandu dengan ukuran kecil, yang mempunyai prestasi unik yang tidak dimiliki oleh pesawat udara yang lebih besar, ia dapat terbang di ruang tertutup dan melakukan aktiviti melayang, penerbangan ke depan dan sebagainya. The Flapping Wing Micro Aerial Vehicle (FWMAV) adalah sejenis kenderaan yang meniru serangga (burung), yang terbang berdasarkan sayap mengepakkan. Berbanding dengan kapal terbang sayap tetap, FWMAV mempunyai banyak kelebihan, seperti saiz kecil, berat ringan, penggunaan kuasa rendah dan kecekapan penerbangan yang lebih tinggi. Sebahagian besarnya boleh digunakan dalam aplikasi ketenteraan dan awam. Oleh sebab kesan ekor, fokus aerodinamik badan kapal akan bergerak di belakang pusat graviti, sehingga dapat stabil secara statik. Pada masa yang sama, sudut permukaan ekor yang berbeza akan menghasilkan masa untuk mengubah sikap terbang FWMAV, dan menjaga keseimbangan yang sesuai. Berdasarkan kajian mengenai mekanisme burung dan serangga terbang, projek penyelidikan ini menunjukkan kawalan sikap penerbangan, sudut antara ekor dan badan, model badan dan ekor. Model kenderaan udara mikro flap yang maju dicipta mengikut prototaip merangkumi beberapa komponen utama iatu sayap, ekor, pesawat, sistem kawalan, struktur mekanik. Kesan orientasi ekor yang berbeza diuji di bawah halaju masuk yang berbeza, sementara itu, untuk mensimulasikan sikap terbang yang nyata, sudut pitch yang berbeza (dari -45°hingga + 45°) pesawat dianggap berdasarkan kaedah ANSYS dan eksperimen sebenar. Setelah membandingkan keadaan yang berbeza, sudut ekor 20 ° yang wajar dipilih dalam projek ini.

Kata kunci: Flapping drone, CFD, Lift force, Tail, ANSYS

ACKNOWLEDGEMENTS

I would like to express my deepest appreciation to all who helped me to successfully complete my research project. I sincerely appreciate my supervisor Dr. Poo Balan Ganesan, who helped me a lot in terms of the professional knowledge and research method. In addition, our project team members Alireza Esmaeilzadeh, and Deng Xinchen who have conveyed some suggestion of experiment and research project. At the same time, a specific mention about my family, they unconditionally support my master study and often encourage me. Many thanks to my friend Chin Ket Vun who had taught me about basics of research. Furthermore, special thanks to the faculty of engineering in University of Malaya (UM), which has provided me a lot of knowledge that can help me in the future career.

TABLE OF CONTENTS

LIST OF FIGURES

LIST OF TABLES

LIST OF SYMBOLS AND ABBREVIATIONS

δ	:	Blockage ratio
S_n	:	Frontal area of the object
S	:	Cross section of the wind tunnel
H	:	Height of model
W	:	Width of model
L	:	Length of model
H'	:	Height of Virtual Wind Tunnel
W'	:	Width of Virtual Wind Tunnel
L'_l	:	Length of left side of the Virtual Wind Tunnel
L'_r	:	Length of right side of the Virtual Wind Tunnel
X	:	Rectangular space coordinates X
Y	:	Rectangular space coordinates Y
Z	:	Rectangular space coordinates Z
u	:	Velocity components of the particle in X axis
v	:	Velocity components of the particle in Y axis
w	:	Velocity components of the particle in Z axis
MAV	:	Micro Aerial Vehicle
Re	:	Reynolds Number
FWMAV	:	Flapping Wing Micro Aerial Vehicle
ρ	:	Density of the fluid (air)
L	:	Total length of the body and tail (body+ tail)
μ	:	Dynamic viscosity
V	:	Maximum velocity of the MAV (Inlet velocity)
P	:	Pressure

v	:	Velocity of fluid (air)
C_L	:	Lift coefficient
A	:	Projected area
t	:	Time
F_x	:	Volume forces of the fluid unit in the x direction
τ_{xx}	:	Components of the viscous force on the fluid element unit surface
FDM	:	Finite-Difference Method
FEM	:	Finite-Element Method
FVM	:	Finite-Volume Method
RANS	:	Reynolds Average Navier-Stokes

LIST OF APPENDICES

CHAPTER 1: INTRODUCTION

1.1 Project background

The Micro Aerial Vehicle is one type of unmanned aerial vehicle with a small size, which has a unique performance that larger aircrafts do not have. MAV can fly in confined spaces and perform hover, forward flight(Nedunchezian, Kang, Aono, & Vibration, 2019). The Micro Aerial Vehicle (MAV) plays a very important role in many respects. Although MAV has a lot of advantages, this kind of vehicle is still facing many problems that are stability, control, weight, material selection(Trizila, Kang, Aono, Shyy, & Visbal, 2011). There are different types of MAV such as fixed-wing, rotary-wing, and flapping-wing (Anderson, 2011). With the development of the MAV, the size of the MAV becomes smaller, in the meantime, the fixed-wing has the problem of the flight attitude control and lift force(Shyy et al., 2010). The flapping drone in this project is a type of flapping wing micro aerial vehicle. There are many flapping wing flyers in nature, some of them with tail, and some of them flying without the tail. The motion of the flapping wing is around the axis of the direction of the flight(Michelson & Reece, 1998). The tailed vehicles can offer more static and dynamic stability. Besides this, it can offer simple control mechanisms that fulfill the requirement of the change of yaw angle and stability(Armanini et al., 2019). To compare with the tailless vehicles, the angle between tail and body of the tailed vehicles need to be considered, because different angle can perform different flight attitude. A tailed vehicle is used in this research project in order to perform well and achieve stability. This project is about to develop and produce a micro air vehicle based on the flapping wing that can fly independently in a normal environment. The lift generated by the limited surface area of the wing and the tail can change flight direction. Unique think about flapping drone is that it can perform take-off, change yaw angle, avoid obstacles and the battery can last around 8 minutes.

1.2 Problem statement

In this project, the prototype is a tailed flapping drone. The investigation of the tail is the most important part in this study. The different angles of the tail can produce different lift and drag which can influence the flight attitude of the flapping drone. The problem in this research project is that the effect of the tail during the flapping process of the wing. And to explore a reasonable angle of the tail to obtain suitable lift and drag to achieve the good performance of flight attitude. In the meantime, we should consider the airflow from the flapping wing and decide the type of airflow. The below Figure 1.1 shows the process of the motion of the wing.

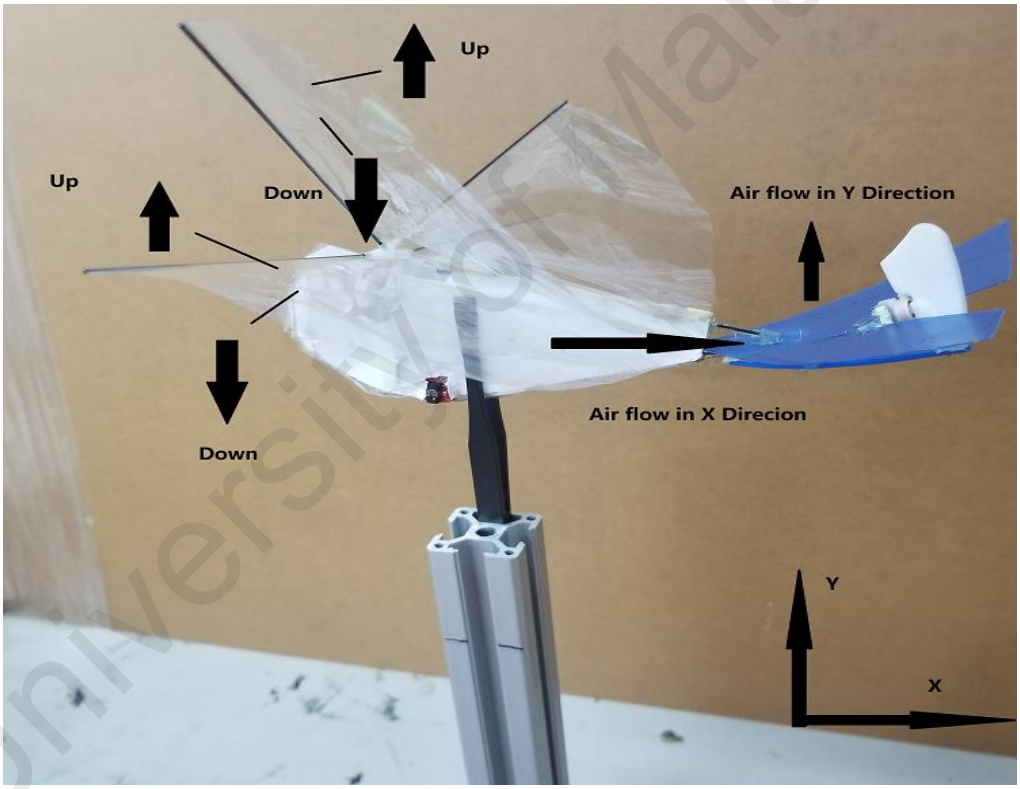

Figure 1.1:Process of the motion of the wing

1.3 Project objectives

The objectives of this study include:

i. To research the drag force and lift force of the model tail and angles using CFD.

ii. To investigate the performance of flight under the modified tail condition.

1.4 Project scope

This research project belongs to fluid mechanics, and it also meets the range of low Reynolds number and incompressible fluid. The project is based on ANSYS software, there are four different models with three types of grids to be considered in a computational domain with suitable blockage ratio to simulate the real flight environment as much as possible. Therefore, the scopes of this research project include:

i. To research the tail part of the prototype of flapping drone.
ii. To carry a basic CFD investigation to measure lift and drag force generated.
iii. To carry a basic testing on flight performance.

1.5 Report outline

This research project included five chapters. The first chapter introduced some basic information about the micro air vehicle based on the flapping wing. The first chapter also introduced the main goal is to explore the reasonable angle of the tail to obtain suitable lift and drag to achieve the good performance of flight attitude. Chapter 2 introduced the development progress of the MAV and FWMAV (flapping drone) and some relative research about the tail of the flight. The third chapter is the methodology, which designed a suitable computational domain with a reasonable blockage ratio and included the information about the ANSYS as well as experimental works. Chapter 4 is about the results from the ANSYS and actual experiment. In chapter 4, the results included the pressure distribution on the tail and the airflow velocity profile around the body and tail. In addition, chapter 4 also listed the information about the actual testing of the model we built in this project. Chapter 5 introduced some findings in this research project and listed some future works.

CHAPTER 2: LITERATURE REVIEW

2.1 Natural flyers

The insect flights and bird flights fly by flapping wing, these are two main types of flapping wing flights in the world (Shyy et al., 2008). Thus, there are also two main types of FWMAV, which are entomopters and ornithopters(Lankford, 2018). The flying mechanisms of insects are different from birds(Biswal, 2015). The wing of the insect flight has three degrees of freedom, and bird flights only have two degrees of freedom(C. T. Orlowski & Girard, 2012). There are many flapping-wing flyers in nature, some of them with tail, and some of them without the tail. For flapping wing flyers in nature, wings are the most important organ. Because wings will bring the necessary thrust and lift during flight. The human realized the flapping wing can produce the lift, drag, and thrust due to the observation of the birds(Rozhdestvensky & Ryzhov, 2003). The flight process of the bird includes: lift force, thrust, drag force and gravity. The drag force parallels to the incoming flows. The direction of the thrust is the same as the direction of flight. The lift force from the flapping-wing is perpendicular to the incoming flows. The steering of bird flight is not relying on the deflection of the tail. The steering is relying on the balance of the body and adjustment of the flight speed. However, the current flapping-wing aircraft cannot completely imitate the flapping-wing bird, because the wing of the bird is highly flexible. In the actual prototype of the flapping-wing aircraft, the tail plays the role of attitude balance, flight direction control and additional lift during the flight of the aircraft.

2.2 Flapping Wing Micro Aerial Vehicle

Unmanned Air Vehicles (UAV) have the potential to completely change the current state of the civilian and military markets(Fenelon, Furukawa, & Theory, 2010). There are so many unique functions on the UAV, the modified drones can be used to help human to observe crops, monitor the environment, and spray pesticides. In the military market,

UAV can be used for intelligence surveillance, enemy surveillance, and reconnaissance. At the same time, drones can also replace people to complete dangerous operations and other tasks. With the development of electronic technology and composite material performance, small unmanned aerial vehicles (SUAV) have been invented. Therefore, the size of the UAV is getting smaller, the lift and thrust force values generated by the flapping wing is getting smaller as well(Abas, Rafie, Yusoff, & Ahmad, 2016). In the 1990s, the United States defined the concept of Micro Aerial Vehicle (MAV) and carried out a series of related research, which pushed the rapid development of the FWMAV. The existing small drones include three different drones which are rotary-wing, fixed-wing drones, and flapping-wing drones(Fenelon et al., 2010).

With the exploration and discovery, people invented fixed-wing aircraft by researching the flying attitude of the bird. After the observation and research of the birds and dragonflies, people invented stable and more flexible aircraft. The birds and insects in nature have a more flexible flight attitude and good aerodynamics. Birds can achieve a series of complex movements in the air, such as hovering, forwarding, diving, and pitching, these are not possible for fixed-wing and rotary-wing aircraft. Therefore, people gradually focused on flapping-wing aircrafts. Compared with flapping-wing aircraft, the flight performance of fixed-wing aircraft is relatively poor when the flying area is no large and without high speed. Flapping drone makes full use of the unsteady fluid around the wings through flapping wing motion, which can generate additional lift. Therefore, under the low Reynolds number situation, the flapping drone has more advantages. In addition, the flapping drone has higher flexibility and maneuverability. Some of aircrafts based on the flapping wing can perform short take-off and landing in relative low speed. And some of the flapping drone with enough power and better control system can take off and land vertically(Maglasang, Isogai, Goto, & Yamasaki, 2006). At the same time, flapping drone also cause less noise than rotorcraft with the same size. The adaptability of the flapping

drone is also distinguished under different mission situations. The bionic flapping drone can perform cruising and hovering like the flapping-wing flying creatures in nature. The aerodynamics of the wing is decided by the wing kinematics because the degree of freedom of wings of insects are not same(Biswal, 2015).

2.3 Effect of tail

Although the concept of MAV has been defined for several decades, the current study is still facing many challenges. The reason is that the size of the micro flapping-wing vehicle is too small. The flapping wing micro aerial vehicle and traditional aircraft are different such as theories, technologies, methods, aerodynamics, materials, structure, energy, etc.

Recently, with the development of simulation skills, flapping-wing aircrafts that mimic birds and insects have become one of the focuses of research in different countries. Some related problems of flapping wing micro aerial vehicle have become research difficulties due to the non-linear characteristics as well as complex mechanisms(Armanini et al., 2019). The common problems faced by engineers in flapping wing micro aerial vehicles are unsteady aerodynamics, analog simulation etc. These aspects can lead to different performances in different applications. The problem of a study was to research the unsteady aerodynamics of the flapping drone(Ho, Nassef, Pornsinsirirak, Tai, & Ho, 2003). The Micro Aerial Vehicle is different from the traditional aircraft with high Reynolds Number. Because the flying velocity of flapping drone is relatively low, which means the Reynolds Number is relatively low. The Reynolds Number of the flapping drone is below 10^6 (Tsai, Fu, & Technology, 2009), and some of the insects even have lower Reynolds Number (10^2-10^4) than the flapping drone.

The magnitude of the lift provided by the wing is larger than the lift generated by the tail. Due to the entire surface of the wing part is larger than the surface of the tail.

Therefore, the main role of the wing is to provide the lift for the flapping drones. The lift generated from the tail is almost negligible compared with the lift generated from the wing. Thus, the function of the tail is to control the flight attitude in most cases. On the other hand, the tail with a certain angle can offer force, because the airflow generated from the flapping wing will act upon the surface of the tail. In the meantime, the aerodynamic force on the tail is far away from the mass center of the flapping drone. Therefore, the tail can generate a larger force to change the direction of the head of the flapping drone. In this project, the main role of the tail is considered to control the pitch angle and yaw angle of the flapping drone. Besides, the aerodynamic focus of the body(fuselage) will move behind the center of gravity due to the effect of the tail, so that it can be statically stable and maintain a corresponding balance(Armanini et al., 2019). The flapping drone with a tail has good maneuverability, hover capability, and lift generation. Compared with traditional aircraft, the tail of a traditional aircraft is used to balance torque, maintain stability, and improve maneuverability, so they have very similar functions.

The vertical rudder deflection can influence the yaw angle of the flapping drone. The rudder of the flapping drone is a kind of drag rudder, which can adjust the frontal area to generate different force to change the flight attitude(Z. Zhang, Li, Li, & WANG, 2010). Since the flapping drone is too small and light, the rudder that can be installed is limited. Both yaw angle and pitch angle are important to the drone. However, in order to match its limited conditions, the rudder can only be used to change the yaw angle of the flapping drone in this project. But we want to have some pitch angle on the flapping drone. In this case, another reasonable method is the adjustment of the motor speed. The flapping drone can have a reasonable lift, drag, and pitch angle through the adjustment of the motor speed. The motor can be controlled by the controller to obtain different motor speeds to change

the frequency of the flapping wing. In addition, the motor can control the process of the landing of the flapping drone through different motor speeds.

2.4 Previous research

Before the flapping wing micro aerial vehicle, humans had always imitated birds, they used bird feathers to make wings and then used the wing to imitated flight(McMichael, 1997). After numerous failures and attempts, people discovered that the flight of birds cannot be achieved only by feathers. Therefore, people have focused their research on the wing mechanism and did a lot of experiments. After a lot of experiments, the model of flapping-wing aircraft has been gradually invented(Hall & Hall, 1996). As early as the end of the 15th century, a famous Italian painter and engineer called Leonardo da Vinci designed a flapping-wing aircraft powered by manpower. Although it failed to fly, it provided a reference for the design of subsequent flapping-wing aircraft. The below Figure 2.1 shows the ornithopter design("Leonardo da Vinci's ornithopter design.,").

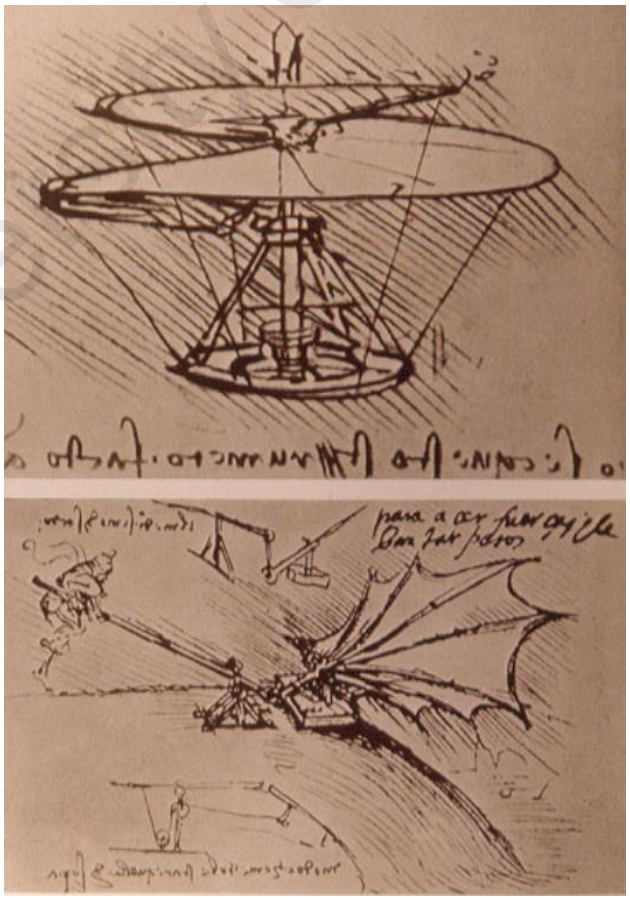

Figure 2.1:Design of the manpower ornithopter

On December 7th, 2000, in the USA, T. Nick Pornsin-Sirirak team redesigned a Battery-Powered Ornithopter with Radio Control System, which is lighter, stronger, and more aerodynamic. The material of the structure of body is carbon rod, the tail is made of plastic foam sheet. During the first flight test of prototype, the drone flew under radio control, where the pilot could control the yaw angle, pitching angle. The below Figure 2.2 shows the Radio Control Ornithopter by T. Nick Pornsin-Sirirak team(Pornsin-Sirirak, Tai, Ho, & Keennon, 2001).

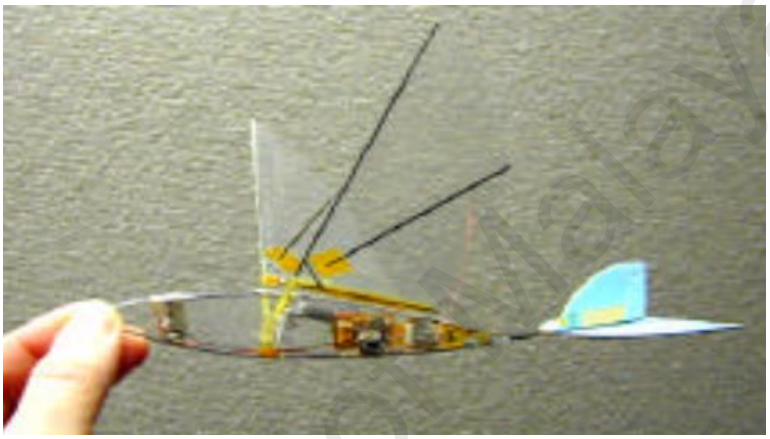

Figure 2.2:Radio Control Ornithopter

The team of Technical University of Delft developed Delfly I, the Figure 2.3 below shows the Delfly I("Delfly I,"). The weight of Delfly I is 3.07g and the wingspan is 10cm(De Croon, De Clercq, Ruijsink, Remes, & De Wagter, 2009). The material of the wing is mylar foil, and the wing flapping frequency is 30HZ("Delfly I,").

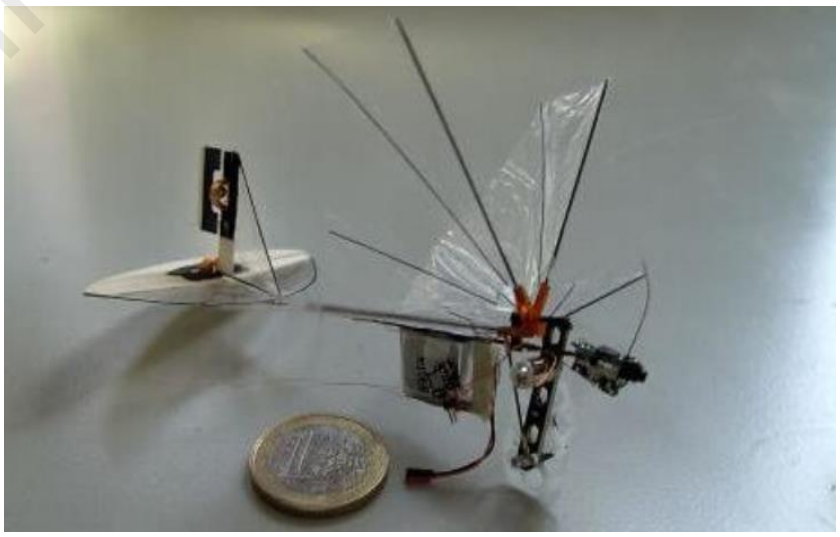

Figure 2.3:Delfly I by Technical University of Delft

The tail plays a significant role in the flapping drone. For example, the aircraft called Smart Bird developed by the German Festo company imitates the shape of a seagull and designed a polyurethane foam material inverted V-shaped movable tail in 2011(Send et al., 2012). The below Figure 2.4 shows the Smart Bird("Smart Bird by Festo company,"). It has a very exquisite control system, both head and tail can swing. It has two modes of remote control and automatic flight, capable of autonomous take-off, maneuver, and landing. The head of the aircraft can realize the adjustment of the flight direction and its own balance because the tail can move and with different deflection angles. The tail has a certain degree of flexibility. It has a stabilizing effect during the flight. In the meantime, due to the use of ingenious structure, the tail surface can carry out small-angle pitch and yaw motions, thus this aircraft can achieve flight control.

Figure 2.4:Smart Bird by Festo company

2.5 Research gap

In 2010, a paper researched to avoid the unstable longitudinal oscillation situation on the FWMAV by two open-loop methods. In the meantime, through the control of the tail and mass to overcome the unstable pitch motion(C. Orlowski, Girard, & Shyy, 2010). In 2012, Yang and Li did a research for the aerodynamic force of the horizontal tail in the

steady and unsteady state. That study used dynamic mesh technology to obtain high mesh quality of unsteady motion and indicated the results from two different states are very different. Yang and Li also stated that the unsteady motion of the flapping wing is very important for the horizontal tail(Yang & Li, 2012). Another previous study predicted the time-resolved aerodynamic force of the tail of flapping drone under the influence of the wing wake(Armanini et al., 2019). That study described the low field around the wake through the PIV method and calculated the conditions of airflow at the tail. That study also explained the reason for the high efficiency of the tail. A next research article compared the hover control performance between the different shape of the tail of a flapping flight. From their study, the tail plays very important role on the pitch angle, yaw angle, lift and drag. Furthermore, they designed a tail with two rudders which can perform better maneuverability. Thus, the investigation of the tail angle is important(P. Zhang, Zhu, & Zhu, 2020).

In conclusion, the focus of this research: the tail part of the flapping drone; the testing of the performance of flight under modified tail condition. Compared with the listed previous studies, the ANSYS model did not include the flapping wing part in this project. We regarded the airflow from the flapping wing (inlet surface) as the unsteady incompressible flow. This project did not use dynamic mesh technology in the MESH part. Moreover, the actual experiment did not include the measurement of the lift(drag) and cl(cd). This was because of the lack of relative measuring instruments. Base on the design of the tail and body, we measured the wind velocity of the tail with a high accuracy velocity meter. And compared the actual value with the simulation value. Due to the effect of the tail, we set one vertical rudder to change the yaw angle. Besides this, we set a certain tail angle to obtain the balance and offer the negative lift force to improve flight performance.

CHAPTER 3: METHODOLOGY

This part is about the methodology that described three aspects that are: tail, CFD, and experimental works. These three aspects show that the development of theoretical knowledge of CFD of the flapping drone, and some details in experimental works.

3.1 Design of the tail

The tail is a very important component of the flapping drone according to the first two chapters. The flying creatures can change the flight attitude through the balance of the body and wing, they also can adjust the flight attitude by the change of the flying speed. Therefore, the tail of the flapping drone became an important method to change the flying attitude. The following chapter 3.1.1 and 3.1.2 listed some details about the type of tail and angle of tail.

3.1.1 Type of the tail

There are three types of the tails, which are sector tail, horizontal and vertical tail, V tail. The detail is given by the below Figure 3.1.

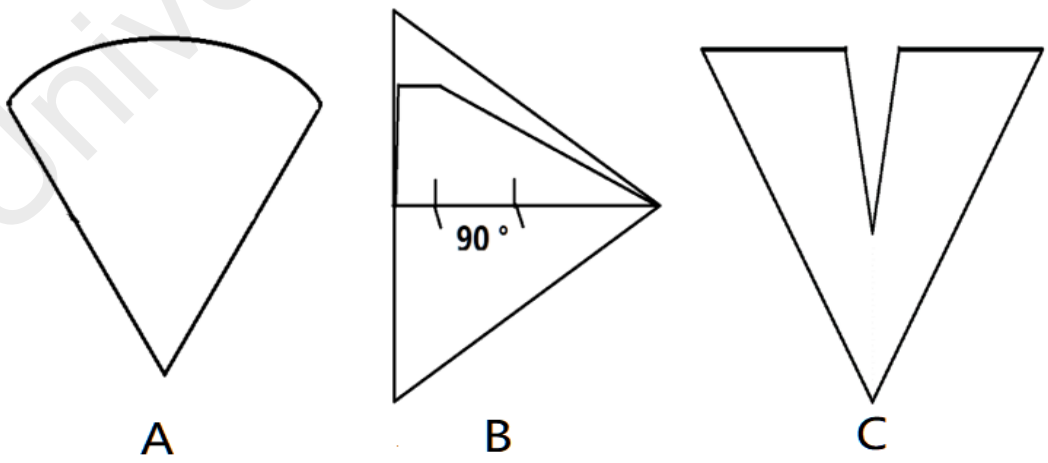

Figure 3.1:Different shapes of the tail

In order to change the yaw moment, the rudder will be used in the tail. From the above three structures (A, B, C), the combination of the B and the C is used. The combination of the tail structure is shown in below Figure 3.2. This method is easy to set light rudder and decrease the total weight of the tail. In theory, more rudders can offer more kinds of flight attitudes(Gerdes, 2010). The aim of this project is to design a small size drone that matched a low power motor. At the first stage, we just set one rudder on the tail due to the low flapping frequency of the wing. Thus, we need to consider the angle between the body and tail to achieve the desired flying attitude in the following step. Appendix A shows the detail of the tail.

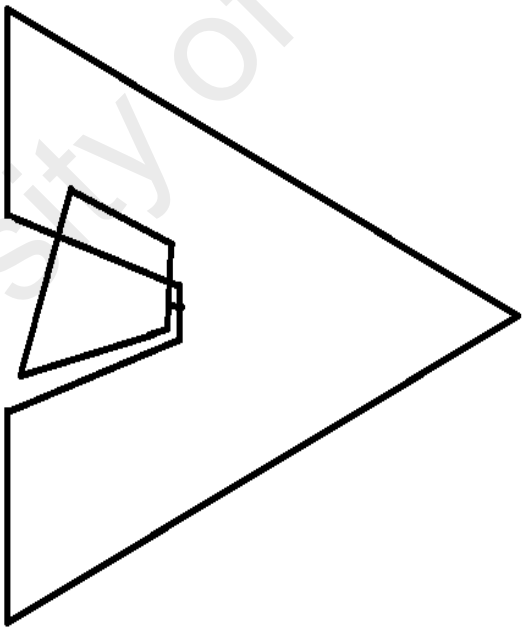

Figure 3.2:Tail Configuration in this project

The subject of this research is to understand the relationship between the body and tail of a flapping drone. In order to explore the effects of angle, we will design four different tail angles to test the performance. The below Figure 3.3 shows the assembly angle of the tail in this project. The adjustment of the angle is dependent on the body size & weight & CG and the tail size. If the tail assembled parallel to the body (0°), all the air will pass through the tail surface and there are no negative lift forces, the drone's head will go down and definitely crash the ground. On the other hand, if the tail has the angle more than 0°, in this case, more wind will push the tail down, therefore the drone's head will go upward. In order to investigate the angle of the tail, the four different angles of the tail are 0 °, 10°, 20°, and 30° respectively.

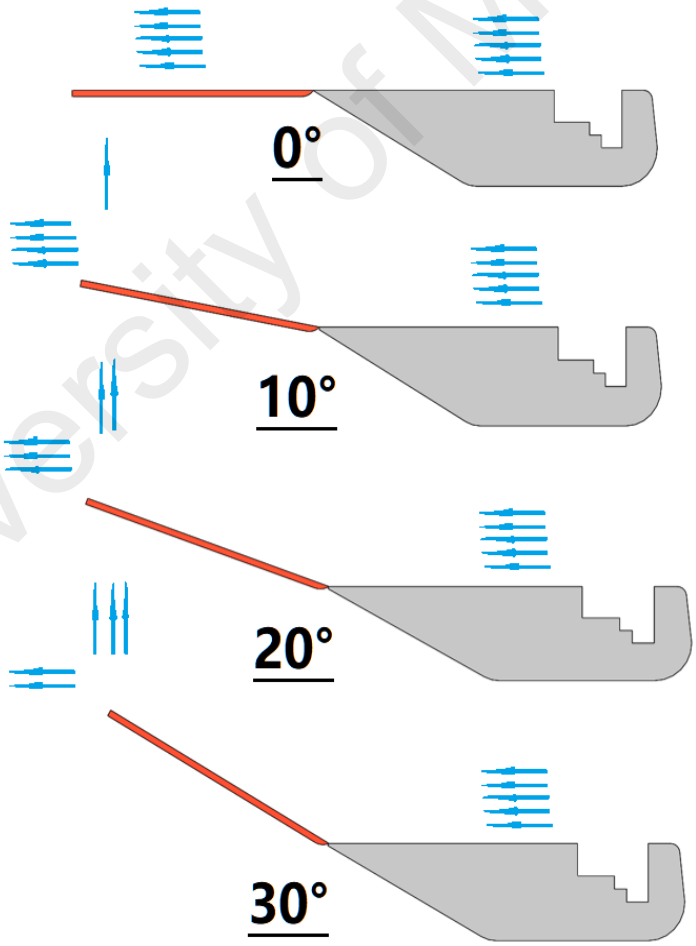

Figure 3.3:Assembly angle of tail

3.2 CFD

The full name of CFD is Computer Fluid Dynamic Analysis. CFD belongs to the fluid mechanics that can analyze and solve fluid problems through the numerical analysis and data structures(Çengel & Cimbala, 1996). The medium around the flapping drone is air(fluid) in this study. For the CFD simulation, the first part is Pre-processing that includes geometry, equations, boundary conditions; The next part is to generate the grid that is a set of control volumes; Then, the solving process is to discretize the governing equations. The next part is Post-processing that is result includes forces, flow rates, etc. Then we can see the desired graphs and plots(Atmaca, Çetin, & Yılmaz, 2019).The below Figure 3.4 show the flow char of the CFD.

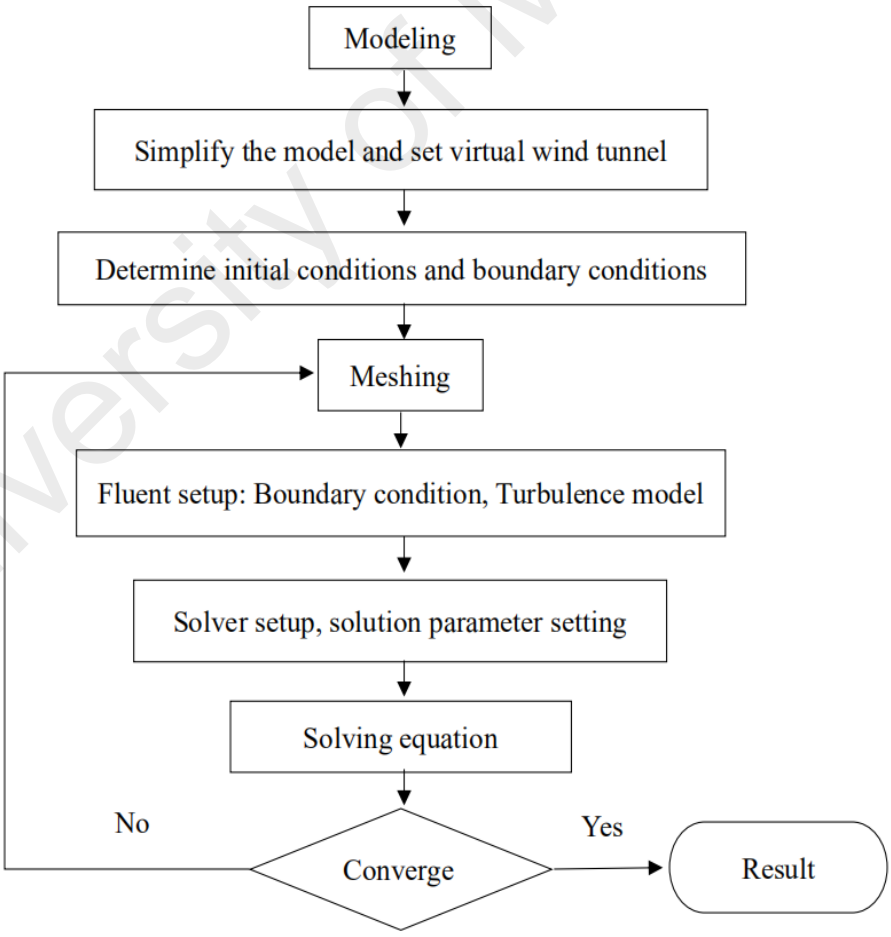

Figure 3.4:Flow chart of the CFD simulation

3.2.1 Reynolds number

The Reynolds number is a kind of dimensionless number and it can reflect the different flow under the different fluid flow situations. The Reynolds number can be expressed by inertial forces divided by viscous forces. Due to the relatively low flight speed and small size of the flapping drone, the Reynolds number is relatively low. Under the low Reynolds number situation, the fluid will generate a large viscous force, which is larger than the inertial force. This can ajust the disturbance of the flow field. In such case the flow field is more stable and appears as laminar flow. If the Reynolds number is relatively high, the viscous force generated by the fluid is small, and its value is smaller than the inertial force. The flow field is unstable due to the inertial force and appears as a turbulent flow. In a word, the Reynolds number is very important to the aircraft's aerodynamic performance. The below Equation 1 shows the Reynolds number equation:

$$\boldsymbol{Re = \frac{\rho V L}{\mu} = \frac{V L}{\nu}} \qquad \textbf{Equation 1}$$

Where: ρ is density of the fluid (air in this project), the unit is kg/m^3; L is a characteristic linear dimension, the unit is m; μ is the dynamic viscosity, the unit is N·s/m^2; V is the fluid velocity, the unit is m/s; ν is the kinematic viscosity of the fluid, the unit is m^2/s. For this project, the temperature at 15℃ is considered. According to "Properties of air at 1 atm pressure" table can know that density of air is 1.225 kg/m^3, kinematic viscosity of air is 1.46×10^{-5} m^2/s. In this project, the Reynolds number is relatively low and maximum value is less than 35000. For the flapping drone, the incompressible fluid around the flapping wing is considered, which means the density ρ of fluid is constant. During the whole process, the heat can be ignored. Therefore, segregated solver is used in FLUENT.

3.2.2 Geometry/CAD model

The first step is to build the model of the flapping drone. For the modeling part, there are much different software that can build the model. We can build the model in the ANSYS software, SolidWorks software, etc. The focus of this project is to analyze of body and tail of a flapping drone. So, the model of the flapping drone is not very complex. We built the model in the ANSYS software. In order to present more details of the assembly of the tail on the body. We built the 3D model in SolidWorks as well. The below Figure 3.5 shows the model (CAD) design in the SolidWorks software. The Appendix A shows the detail of the assembly body.

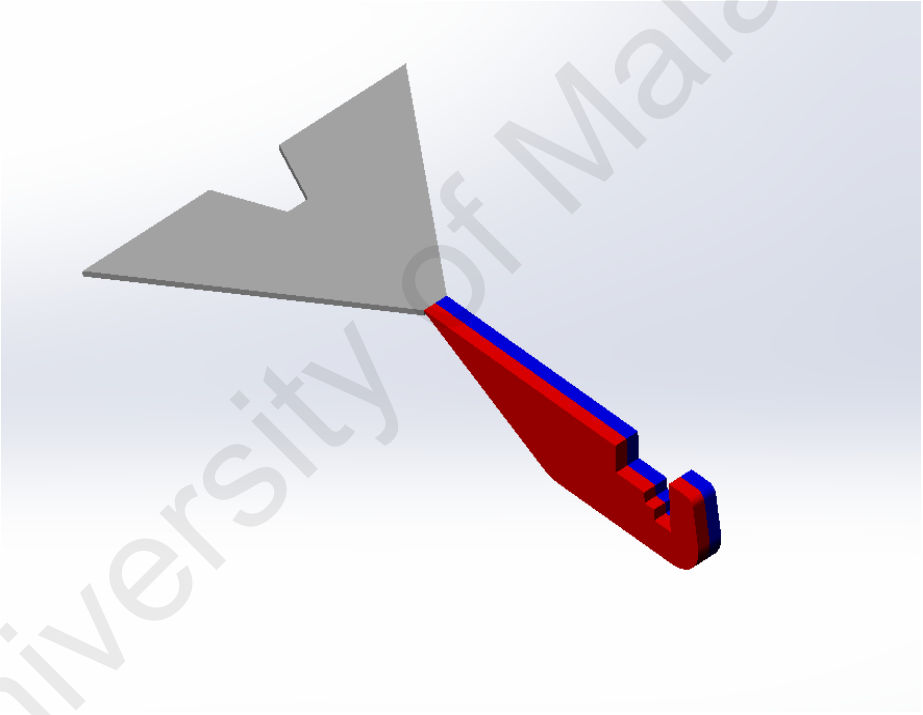

Figure 3.5:SolidWorks model

The Figure3.5 above is just for the 0° angle between the tail and body. Because the angle of assembly of the tail on body has significant effect on the flying condition of the drone. A simplified model with different tail angle was built in ANSYS Geometry. Figure 3.6 shows the ANSYS Geometry model. For the actual model, the wing will be set upward of the body. And the wing surface can cover the area where we set the motor. Thus, we ignored the motor area in the ANSYS model part.

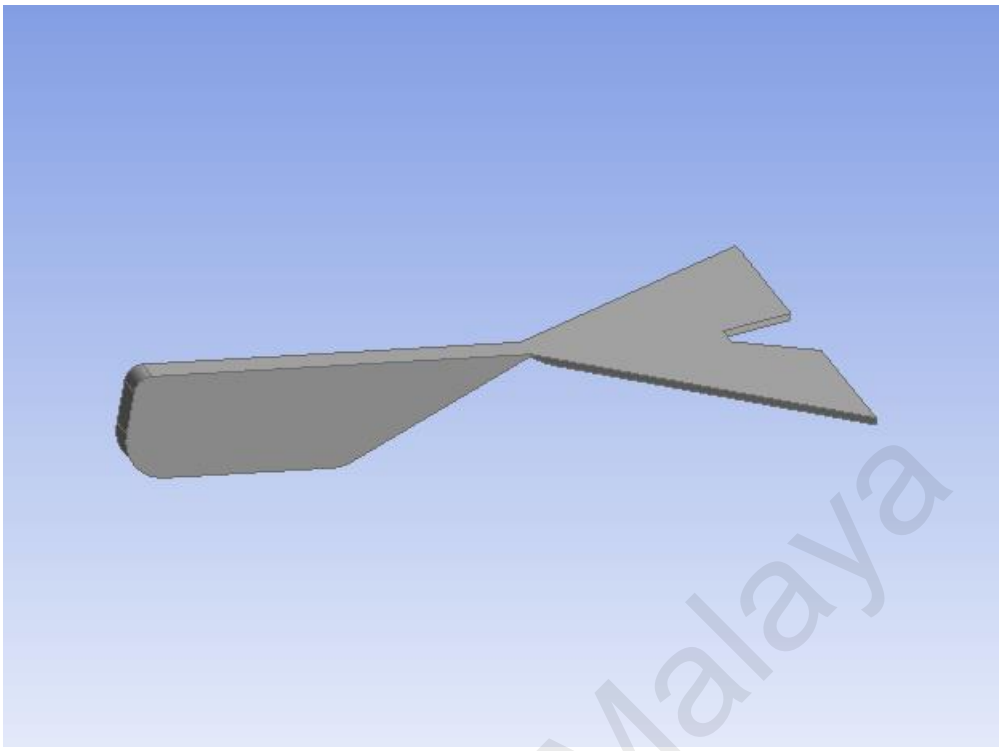

Figure 3.6:ANSYS Simplified Model

3.2.3 Virtual wind tunnel (computational domain)

In general, the wind tunnel can help to research the relationship between the solid objects and the air around the solid objects(Sahini, 2004). In this project, we used a virtual wind tunnel that is a kind of computational domain to simulate the actual flying environment of the flapping drone. The type of wind tunnel is a low wind velocity tunnel since the flapping drone with a maximum of 6 m/s flying velocity. The correct size of the wind tunnel is very important, which can influence the result of the simulation. If the computational domain is too large which needs a more powerful processer of the computer to calculate. Besides this, it also needs more simulation time and calculation steps. The wind tunnel size is according to the size of the flapping drone, which can influence the wind tunnel blockage ratio. Because the blockage ratio is equal to the frontal area divided by the cross-section area of the wind tunnel. The frontal area depends on the size of the model. In general, the blockage ratio cannot be very large. Because the large

blockage ratio will lead to errors and does not correspond to the actual condition(Sahini, 2004).

$$\delta = \frac{S_n}{S} \qquad \textbf{Equation 2}$$

Where δ is the blockage ratio, S_n is the frontal area of the object, S is the cross-section of the virtual wind tunnel. The blockage ratio cannot be very big(Altinisik, Kutukceken, & Umur, 2015). In this project, the model size has height H, width W, and length L. According to the situation of the size of the flapping drone model and the computer performance, we designed the dimension of the computational domain were: The length of the computational domain was 5 times H; The width of the computational domain was 10 times W; The length of the "Left side of the model" was 2 times L; The length of the "Right Side of the model" was 6 times L. The below Table 3.1 shows some details of size of the flapping drone. The below Table 3.2 provided clear details of the size of the virtual wind tunnel. The below Table 3.3 provided blockage ratio details of flapping drone with different tail angle and pitch angle.

Table 3.1:Size of flapping drone

Type	H	W	L
Distance	30mm	127.6mm	198.82mm

Table 3.2:Size of the virtual wind tunnel

Type	H'	W'	L'_l	L'_r
Distance	500mm	1276mm	397.64mm	1192.92mm

Table 3.3:Blockage ratio in different tail angle and pitch angle

Tail Angle	Pitch Angle	cross section(m^2)	Frontal Area(m^2)	Blockage ratio
0° Tail	-45	0.638	0.00857895	1.34%
	-10	0.638	0.00340033	0.53%
	-5	0.638	0.00252746	0.40%
	0	0.638	0.00218736	0.34%
	5	0.638	0.00444665	0.70%
	10	0.638	0.00288353	0.45%
	45	0.638	0.00835554	1.31%
10° Tail	-45	0.638	0.00847607	1.33%
	-10	0.638	0.00484789	0.76%
	-5	0.638	0.00402991	0.63%
	0	0.638	0.00322556	0.51%
	5	0.638	0.00254094	0.40%
	10	0.638	0.00504618	0.79%
	45	0.638	0.00645868	1.01%
20° Tail	-45	0.638	0.00884097	1.39%
	-10	0.638	0.00551222	0.86%
	-5	0.638	0.00470366	0.74%
	0	0.638	0.00458491	0.72%
	5	0.638	0.00365666	0.57%
	10	0.638	0.00360445	0.56%
	45	0.638	0.00586351	0.92%
30° Tail	-45	0.638	0.01031848	1.62%
	-10	0.638	0.00733535	1.15%
	-5	0.638	0.00596137	0.93%
	0	0.638	0.00517675	0.81%
	5	0.638	0.00473018	0.74%
	10	0.638	0.00381622	0.60%
	45	0.638	0.00437133	0.69%

In Table 3.3, all the blockage ratio of the flapping drone in different pitch angles are less than 2%. This can induce the computational domain is reasonable. This type of virtual wind tunnel can include many pitch angles(positive45°-negative45°) of the fuselage in the future research steps.

3.2.4 Governing equation

In the analysis of fluid mechanics, three basic physical principles need to be met, which are Newton's second law, the law of conservation of mass, and the law of energy conservation. These physical principles can be determined by the three basic governing equations of momentum, continuity, and energy. In this project, the incompressible flow field caused by the process of the flapping wing, which around the body of the flapping drone. And the flow field is also considered to be an isothermal and adiabatic flow, so the energy conservation can be neglected. In terms of low Reynolds Number, the Navier-Stokes equation is widely used in describing the viscous fluid motion of the boundary layer. N-S equation is a very important method to describe the basic mechanical property of the viscous fluid motion.

3.2.4.1 Continuity equation

The continuity equation comes from the principle of mass conservation, in which the mass must remain constant over time and the mass cannot change without any external factor. For the fluid particle, the inflow mass of the fluid particle and the outflow mass of the fluid particle should be equal, which meets the principle of mass conservation. Therefore, the continuity equation is shown in the below Equation 3.

$$\frac{\partial u}{\partial x} + \frac{\partial v}{\partial y} + \frac{\partial w}{\partial z} = 0 \qquad \textbf{Equation 3}$$

Where x, y, z are the rectangular space coordinates respectively; u, v, w are the velocity components of the particle in x, y, z direction respectively.

3.2.4.2 Momentum equation

The momentum equation comes from Newton's second law of motion. The momentum equation requires that the time rate of momentum change in the given direction is equal to the sum of the forces acting in that direction.

$$\frac{\partial(\rho u)}{\partial t} + \nabla(\rho u\vec{u}) = -\frac{\partial p}{\partial x} + \frac{\partial(\tau_{xx})}{\partial x} + \frac{\partial(\tau_{yx})}{\partial y} + \frac{\partial(\tau_{zx})}{\partial z} + \rho F_x \quad \textbf{Equation 4}$$

$$\frac{\partial(\rho v)}{\partial t} + \nabla(\rho v\vec{u}) = -\frac{\partial p}{\partial y} + \frac{\partial(\tau_{xy})}{\partial x} + \frac{\partial(\tau_{yy})}{\partial y} + \frac{\partial(\tau_{zy})}{\partial z} + \rho F_y \quad \textbf{Equation 5}$$

$$\frac{\partial(\rho w)}{\partial t} + \nabla(\rho w\vec{u}) = -\frac{\partial p}{\partial z} + \frac{\partial(\tau_{xz})}{\partial x} + \frac{\partial(\tau_{yz})}{\partial y} + \frac{\partial(\tau_{zz})}{\partial z} + \rho F_z \quad \textbf{Equation 6}$$

Where p is pressure; ρ is the density of the fluid(air); t is time; $\tau_{xx}, \tau_{xy}, \tau_{xz}$ are the components of the viscous force on the fluid element unit surface; F_x, F_y, F_z are the volume forces of the fluid unit in the x, y, and z directions.

3.2.4.3 Turbulence modeling

In this project, the maximum Reynolds number is less than 35000 according to the calculation. The airflow should be laminar flow. But our project is MAV based on the flapping wing, the airflow is generated from the flapping wing and the process of the flapping is upward and downward. Thus, we need to regard the airflow as turbulence. In principle, turbulent flow can be described by Navier-Stokes equations. But during the most solution process, it is not feasible to solve a large range of time and space by direct numerical simulation (DNS). For this reason, the averaging process must be applied to the Navier-Stokes equation. The most widely used averaging process is the Reynolds average equation, which is Reynolds average Navier-Stokes (RANS) method(Alfonsi, 2009). Through this process, the turbulent structure in the flow can be eliminated to obtain the average velocity and pressure. Turbulence flow is a three-dimensional unstable random flow form. Turbulence models are based on the Reynolds average equation and the pulsation equation to establish a set of closed equations describing the average amount of turbulence. The main thing is to express the second-order relation of velocity pulsation as the product of the average velocity gradient and the turbulence viscosity coefficient.

Although the turbulence model based on the Reynolds average equation can only describe the average value of the physical quantities of the flow field, it has been widely used in engineering due to its short calculation time. There are several different turbulence models that can be used. They are zero equation, one equation, two equations, four equations, etc. In airfoil problems and aircraft aerodynamic numerical simulation experiments, the k-ω model, k-ε model Spalart-Allmaras (S-A) model, and Transition SST are often used(Junkui, 2015). In this project, the flow field here is regarded as fully turbulent, the turbulence modeling is standard k-ε model(Nabawy, ElNomrossy, Abdelrahman, & ElBayoumi, 2012).

3.2.4.4 Numerical method

The most important part of the aerodynamics of the aircraft is to solve the governing equations. Partial differential equations are discretized into a system of algebraic equations. All algebraic equations are solved numerically to render the solution field. The numerical method to be used in terms of the N-S equations, which equations are nonlinear. There are some main methods to discretize, which are FDM, FEM, FVM. They can discretize the whole area to calculate easily and can express the differential equations in a simple way as well. Finite-Difference Method (FDM), which is based on the direct approximation of a differential form of the governing equations. It is the earliest method in the CFD. The FDM is very powerful in terms of structured grid rather than unstructured grid. The full name of the FVM is Finite-Volume Method, this method to derive the discrete equation can ensure its conservation characteristics and the clear physical meaning of the discrete equation coefficients. So FVM is often used for flow and heat transfer problems and also popular in Fluent and STAR-CD software. In this project, we used FVM to solve the relative problem.

3.2.5 Boundary condition

The boundary conditions need to be considered in this project, which are inlet surface, outlet surface, symmetry surface, and wall(Lee, Lua, Lu, Aisyah, & Lim, 2016). The body and the tail assembly are symmetry in the XY plane. In order to decrease the mesh generation time and simulation (calculation) time, the symmetry surface is considered. The symmetry surface can reduce the number of grids and improve the calculation accuracy(Mystkowski & Jastrzębski, 2013). The below Table 3.4 shows some details of the boundary conditions. The below Figure 3.7 shows the name section in ANSYS.

Table 3.4:Boundary Conditions

Name	Type	Parameters
Body A	Wall	-
Outlet B	Pressure-outlet	0 Pa
Symmetry D	Symmetry	-
Wall C	Wall	-
Inlet E	Velocity-inlet	2,3,4,5,6 m/s

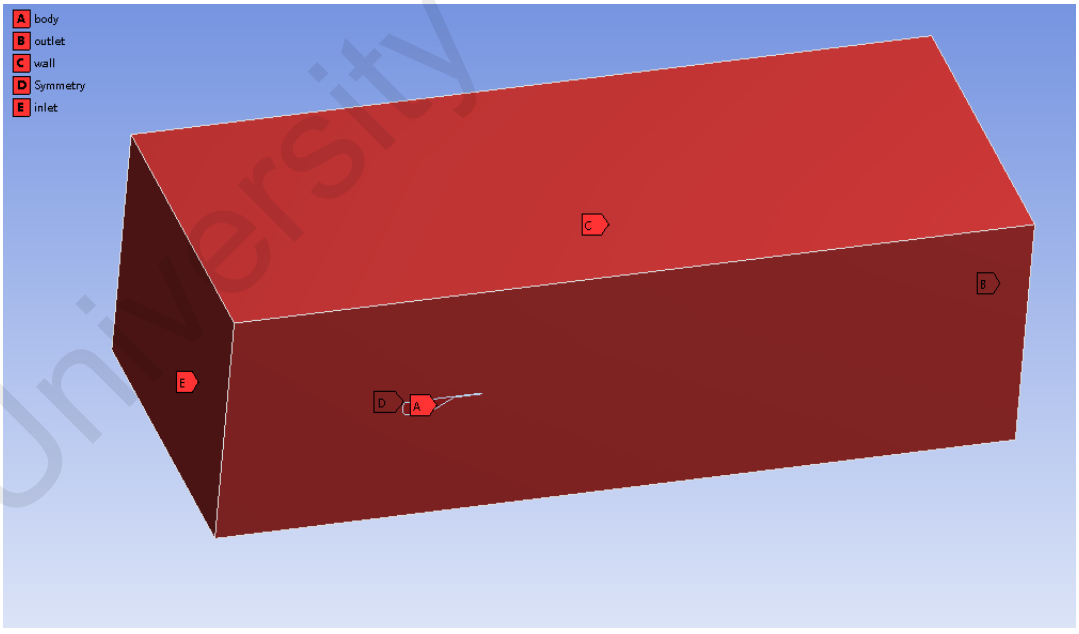

Figure 3.7:Name section

3.2.6 Simulation cases

There are four different flapping drone models in this project. First, four different models were built in “Geometry” module and the symmetry surface was set. Then the established model was imported into “MESH” module to set the grid. In order to ensure

the accuracy of the simulation, three different MESH were constructed to compare the simulation results. Through the inspection of the three types of grid, they all met the requirements of Aspect Ratio, Element Quality, Skewness, Orthogonal Quality, and make sure the minimum volume is positive. After the meshing was completed. Ran the Double-Precision mode FLUENT and selected the standard k-ε for the turbulence model. Then entered the boundary conditions and selected the "simple" solver and the second-order upwind scheme. Then calculate the frontal area. The next step is to set 1000 iteration steps for calculation. With the continuous progress of the convergence calculation process, the solver monitors the residual value gradually converging. The residual represents the satisfaction of the basic mass, momentum conservation equation, and specific turbulence model parameters. The constant residuals can be used as a measure of convergence. Moreover, in order to judge the convergence of the calculation solution, we can monitor the lift, drag, cl, and cd. At the same time, we can also monitor the changes of the temperature, pressure, speed, etc. at a certain coordinate point. When the values from the monitoring points remain unchanged with the iteration continuing, the simulation result can be regarded as convergence.

3.2.7 Mesh independency investigation and validation

The accuracy of the calculation needs denser grids. But this does not meet the actual engineering application requirements. The denser grid means the huge number of grids, which undoubtedly increases the time of analysis and solution of the computer. Moreover, in the actual calculation and application process, the solution accuracy does not increase linearly with the increase of the number of grids. The type of grid should be suitable for actual computing resources. In order to obtain grids that meet the calculation conditions and calculate results that meet the actual conditions, the reasonable control of the

complexity of the geometric model are required. The below Figure3.8 shows one type of mesh.

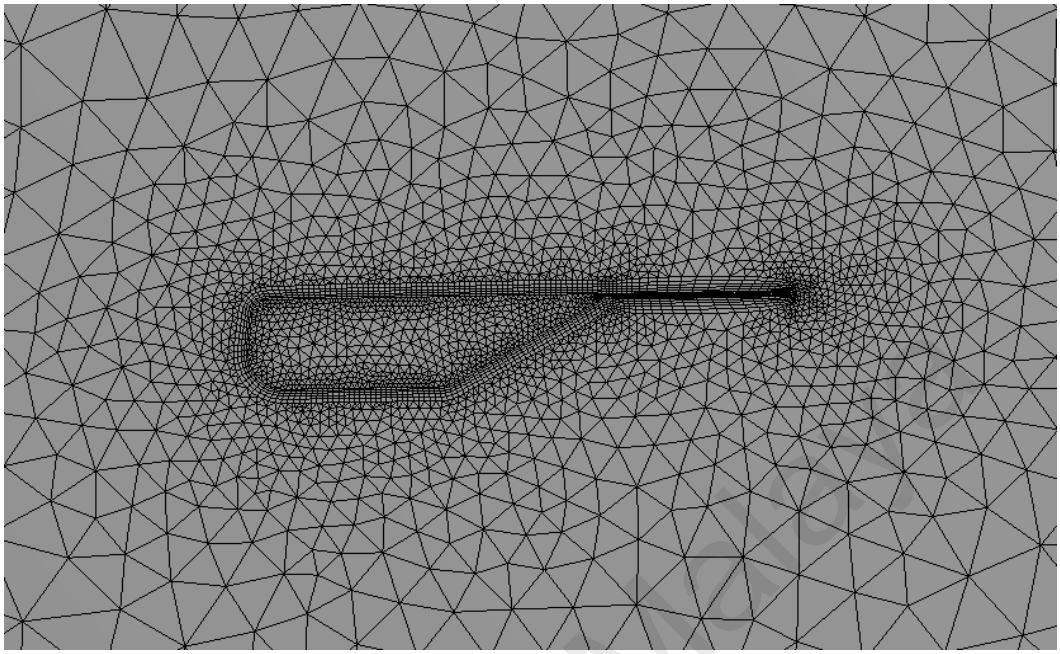

Figure 3.8:Mesh with inflation

The unstructured grids and structured grids are the main grids used in flow field simulation. The structured grid is regular, and with the advantages of simple structure, convenient construction, easy calculation. The disadvantage of the structured grid is it has poor adaptability to complex geometric shapes and has irregular and complex shapes. The structured grid is difficult to meet the special requirements. The unstructured grids do not have the structural limitations of grid nodes, and this kind of grids are easy to control the size, form and node location of grid cells. Thus, the unstructured grids have good flexibility and strong adaptability to the complex shapes. However, the irregularity of unstructured grids also leads to the increase of storage space and addressing time. And this type of grids has low calculation efficiency, long calculation time, and other shortcomings in simulation calculations. Considering the whole surface of the flapping drone model, the unstructured grids are be used(Yang & Li, 2012). The ANSYS Workbench mesh platform is considered in this research project. Compared with other mesh platform, the ANSYS Workbench mesh platform has some advantages. This mesh

platform can check the grid to avoid the appearance of negative volume grids that affect the calculation and solution. Besides this, it can ensure the quality of the grid. The parameterization method can be used to set the mesh size as an independent variable to satisfy the user's requirement. In order to check the effect of mesh refinement and the influence of the grid type on the prediction results, three types of grid details are shown from Table 3.5 to Tale 3.7. Mesh 1-3 is Coarse, Medium, Fine respectively(Harputlu, 2014).

Table 3.5:The drag and lift of Mesh 1

Tail angle	Cd	Drag force(N)	Lift force(N)	Cl	Frontal Area
0°Tail	0.1993842	0.001314761	0.0001512	0.022928861	0.00119621
10°Tail	0.2484771	0.002416177	0.00711204	0.73139453	0.00176398
20°Tail	0.4664781	0.005554869	0.01288207	1.0817906	0.0021602
30°Tail	0.683257	0.009596662	0.01581123	1.1257175	0.00254793

Table 3.6:The drag and lift of Mesh 2

Tail angle	Cd	Drag force(N)	Lift force(N)	Cl	Frontal Area
0°Tail	0.18138344	0.001196062	0.000157	0.023827559	0.00119621
10°Tail	0.23009576	0.002237437	0.006858	0.70523764	0.00176398
20°Tail	0.44794447	0.005334168	0.012691	1.0657749	0.0021602
30°Tail	0.67518222	0.009483248	0.01572	1.1192426	0.00254793

Table 3.7:The drag and lift of Mesh 3

Tail angle	Cd	Drag force(N)	Lift force(N)	Cl	Frontal Area
0°Tail	0.176988	0.001167081	0.000138862	0.021058423	0.00119621
10°Tail	0.232989	0.002265575	0.006914719	0.71110255	0.00176398
20°Tail	0.452322	0.005386292	0.012733982	1.0693544	0.0021602
30°Tail	0.677789	0.009519865	0.015767865	1.1226304	0.00254793

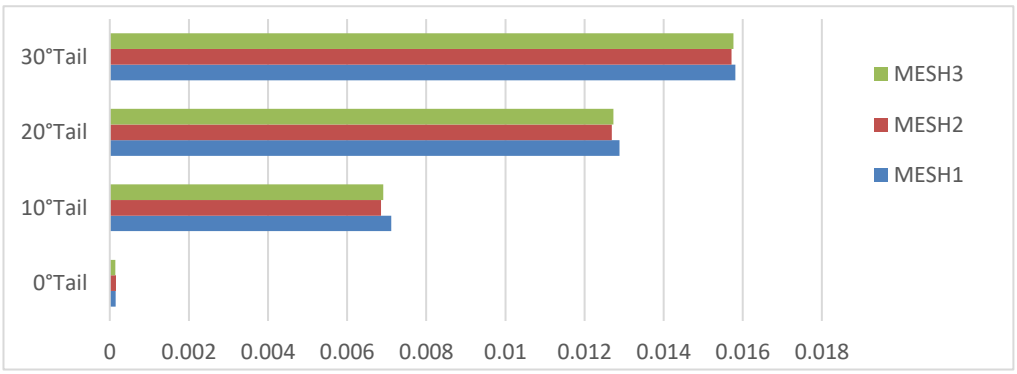

Figure 3.9:Bar chart of negative lift force

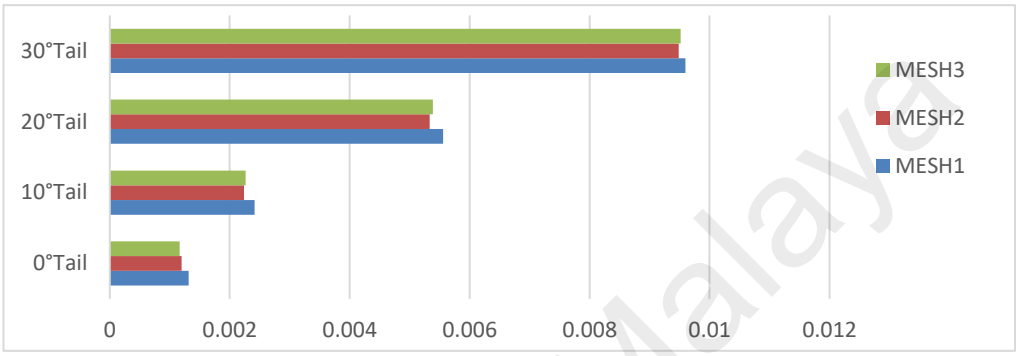

Figure 3.10:Bar chart of drag force

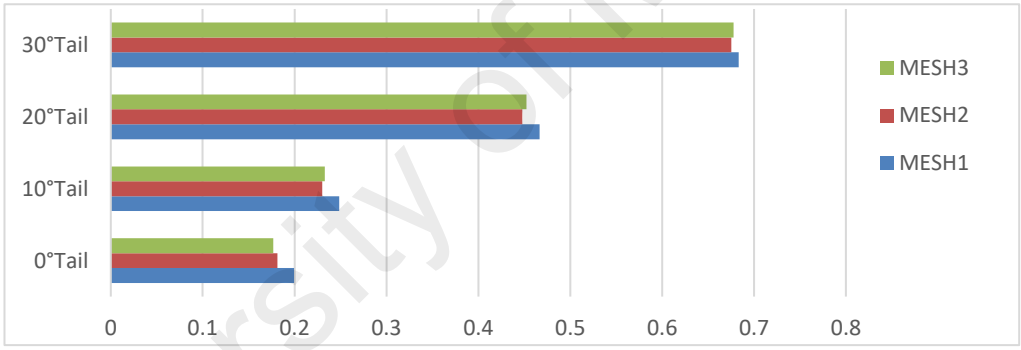

Figure 3.11:Bar chart of cd

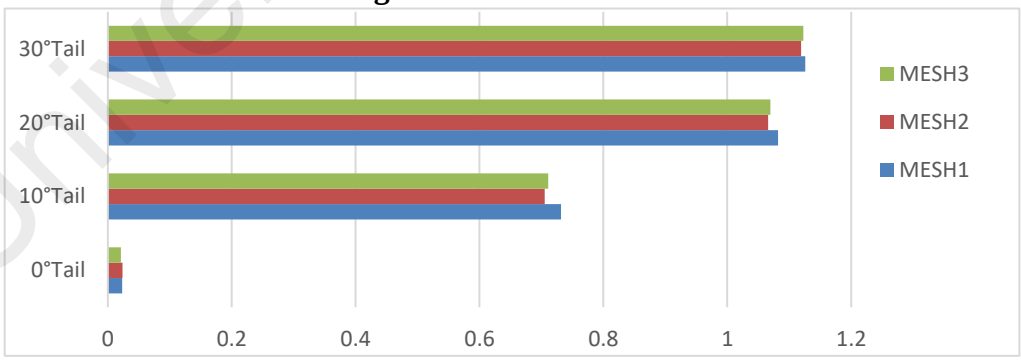

Figure 3.12:Bar chart of cl

From the above Figures, the higher difference value percentage between the maximum value and the minimum value are 2.615% and 2.239%. The rest difference values percentage are less than 2%. From the grid independence test, we can deduce that the medium mesh refinement is sufficient to converge the numerical solutions.

3.3 Experimental works

3.3.1 Measuring equipment

3.3.1.1 Hot wire anemometer

For the flapping drone in this project, there is a very important step is to measure the wind velocity around the tail. Since different areas where around the tail with different velocity, the velocity profile should be measured. In this research project, we collect the data of the wind velocity through the hot wire anemometer. This device is popular in the field of fluid mechanics. This device can measure air velocity, air temperature, and air quantity. The measurement range of the air velocity is from 0 to 30 m/s, which meets the basic requirement of this project. Figure 3.13 shows the device to measure the wind velocity. The Figure 3.14 shows the process of the measurement of velocity profile.

Figure 3.9: Device to measure the wind velocity

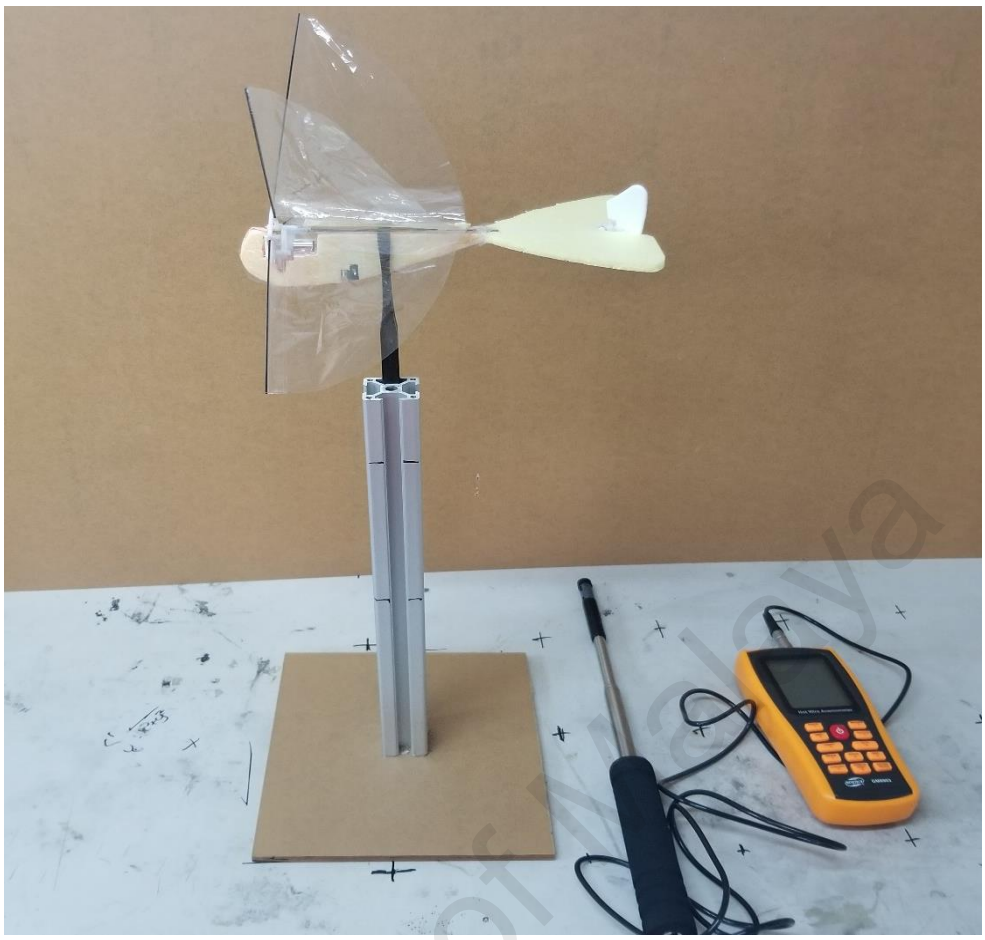

Figure 3.10:Measure the velocity profile

3.3.2 Component product details

The topic of this project is flapping drone, which needs to as light as possible. In order to decrease total weight, the plastic wing, foam body, carbon stick, and foam tail are used in this model.

3.3.2.1 Body

The body is semi bullet shape with 116.12mm length, about 30mm height, and 9mm width. The detail of the last version of the body is shown in the Appendix. Figure 3.14 shows the shape of the body made with Polystyrene Foam. Polystyrene is famous for insulating and lightweight properties.

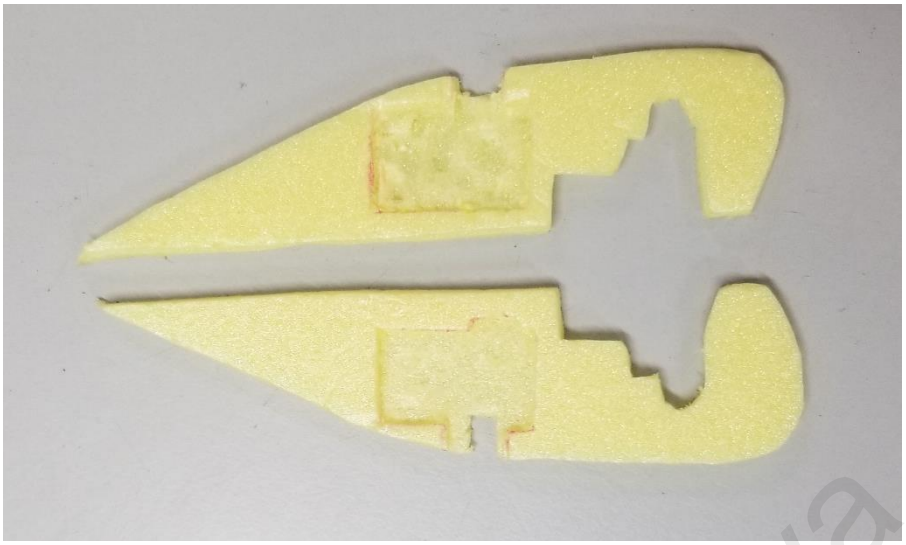

Figure 3.11:Configuration of the body

3.3.2.2 Wing

In this project, we used a kind of very light and soft material to make the wing. The wing material is made up of mylar and the thickness is just 0.05mm. The below Figure 3.15 shows the wing of this project. The wing structure is composed of two parts, which are mylar material and carbon stick (130mm). The detail of the size: the chord length is 280mm, the height is 90mm, the radius is 156mm.

Figure 3.12:Flexible wing

The Figure 3.15 just shows one layer of the wing (wing area is 250cm^2). In this research project, the wing structure includes two layers. The total weight of the wing is 3.48g. The wing part includes two layers wing and carbon stick.

3.3.2.3 Battery

The Li batteries that have been used for the model in this project. This kind of battery has a lot of advantages, which are light and small size. This battery can support power for approximately 8 minutes of flight after full charge. The dimension of the batter is 15mm width, 20mm length, and 7.5mm height. The total weight is around 8g. The price is around 10 RM. The below Figure 3.17 shows Li battery we used in this project.

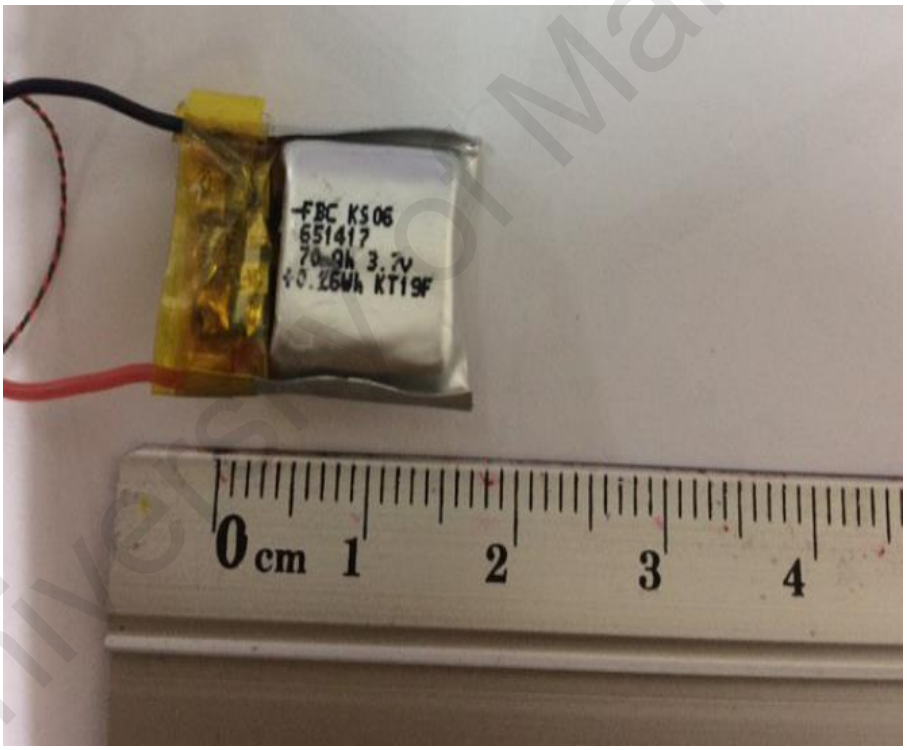

Figure 3.13:Li battery

3.3.2.4 Controller

There are two main components for the flight control system, the ground station and the onboard circuit. The below Table 3.8 shows the specifications of transmitter and receiver with the 2.4GHZ remote control frequency.

Table 3.8:Specifications of transmitter and receiver

Parameters	Specifications
Transmitter	
Working voltage	DC 6V
Using ordinary conventional	4pcs / 1.5V AA battery
Do not use a rechargeable / High alkaline battery (High voltage will damage the circuit board)	
Receiver:	
Working input voltage:	DC 3.2V
lithium battery	3.4 V
The Open environment Remote control distance	80m
The motor connection	M1-, M2-, M+

3.3.2.5 Tail assembly

The tail assembly for this flapping drone model consists of 3 main components of the triangle tail, rudder and magnetic actuator. The tail designed with the isosceles triangle shape. We used high-density polystyrene foam to produce the lightweight tail. The rudder that is a primary control surface used to steer the drone has been produced with high-density polystyrene foam sheet. The weight for latest version is 0.8g. The below Figure 3.18 shows a magnetic actuator can drive the rudder to control the flying attitude.

Figure 3.14:Magnetic actuator for flight control

The electromagnetic actuator has 4.5 mm internal diameter and the maximum size of 11 * 12mm arm length. It is only 0.28g and has 80 ohms resistance and 0.05mm wire diameter and the weight of the tail is 2.6g. The tail assembly with supports material and a magnetic actuator is 5.4g weight.

CHAPTER 4: RESULTS & DISCUSSION

4.1 ANSYS

4.1.1 Drag force and negative lift force

The below Table from 4.1 to 4.4 shows the drag and negative lift under different situation. Figure from 4.1 to 4.4 show the curve graphs of Table 4.1-4.4. The equation 7 and 8 show the relationship between negative lift force (drag force) and lift coefficient (drag coefficient).

$$\boldsymbol{L = \frac{1}{2}\rho v^2 C_L A} \qquad \textbf{Equation 7}$$

$$\boldsymbol{D = \frac{1}{2}\rho v^2 C_D A} \qquad \textbf{Equation 8}$$

Where ρ is the density of fluid (air); v is the velocity of fluid (air); C_L is the lift coefficient at the desired angle of attack; C_D is the drag coefficient at the desired angle of attack; A is the projected area; L is the lift force; D is the drag force.

Table 4.1:Drag, Cd, Negative Lift, Cl under 3m/s inlet velocity

Pitch Angle (°)		Cd	Drag (N)	Negative lift (N)	Cl	Frontal Area(m^2)
0°Tail	0	0.1993842	0.001314761	0.000151	0.022928861	0.00119621
10°Tail	0	0.24847714	0.002416177	0.007112	0.73139453	0.00176398
20°Tail	0	0.46647809	0.005554869	0.012882	1.0817906	0.0021602
30°Tail	0	0.68325703	0.009596662	0.015811	1.1257175	0.00254793

Table 4.2:Drag, Cd, Negative Lift, Cl under 4m/s inlet velocity

Pitch Angle (°)		Cd	Drag (N)	Negative lift (N)	Cl	Frontal Area(m^2)
0°Tail	0	0.18352804	0.002151473	0.000251	0.021413525	0.00119621
10°Tail	0	0.24307775	0.004202086	0.012965	0.75001066	0.00176398
20°Tail	0	0.46794777	0.009906435	0.023452	1.1078115	0.0021602
30°Tail	0	0.68294201	0.017052867	0.028575	1.144369	0.00254793

Table 4.3:Drag Cd, Negative Lift, Cl under 5m/s inlet velocity

Pitch Angle (°)		Cd	Drag (N)	Negative Lift (N)	Cl	Frontal Area(m^2)
0°Tail	0	0.173418	0.003176497	0.000386916	0.02112339	0.00119621
10°Tail	0	0.239928	0.006480693	0.020553437	0.76092998	0.00176398
20°Tail	0	0.468704	0.015503809	0.037192791	1.1243945	0.0021602
30°Tail	0	0.68248	0.026627077	0.045085628	1.155592	0.00254793

Table 4.4:Drag, Cd, Negative Lift, Cl under 6m/s inlet velocity

Pitch Angle (°)		Cd	Drag (N)	Negative Lift (N)	Cl	Frontal Area(m^2)
0°Tail	0	0.16726213	0.004411778	0.000566	0.021462933	0.00119621
10°Tail	0	0.23764176	0.009243257	0.029842	0.76724094	0.00176398
20°Tail	0	0.4694467	0.022360877	0.054113	1.1360476	0.0021602
30°Tail	0	0.68216406	0.038325243	0.065328	1.1628038	0.00254793

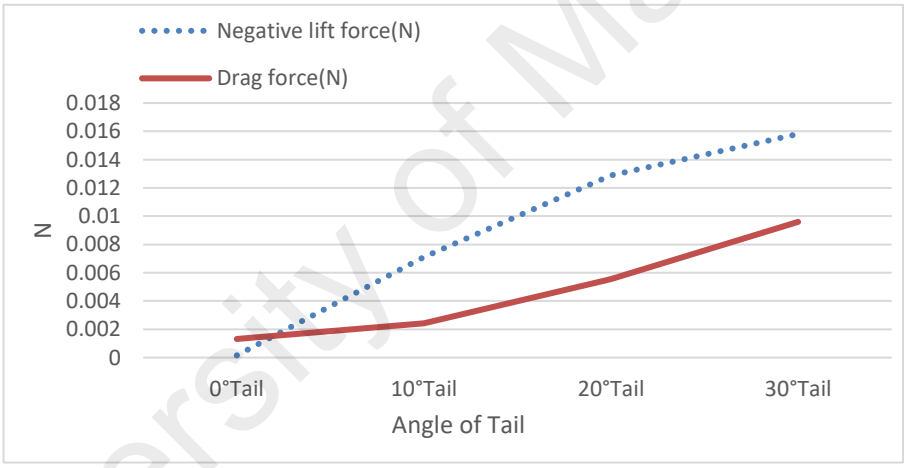

Figure 4.1:Drag, Cd, Negative Lift, Cl under 3m/s inlet velocity

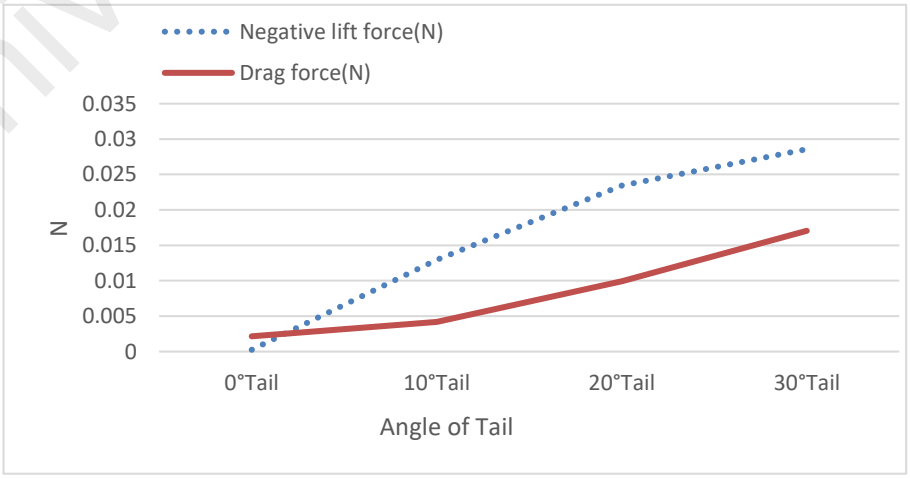

Figure 4.2:Drag, Cd, Negative Lift, Cl under 4m/s inlet velocity

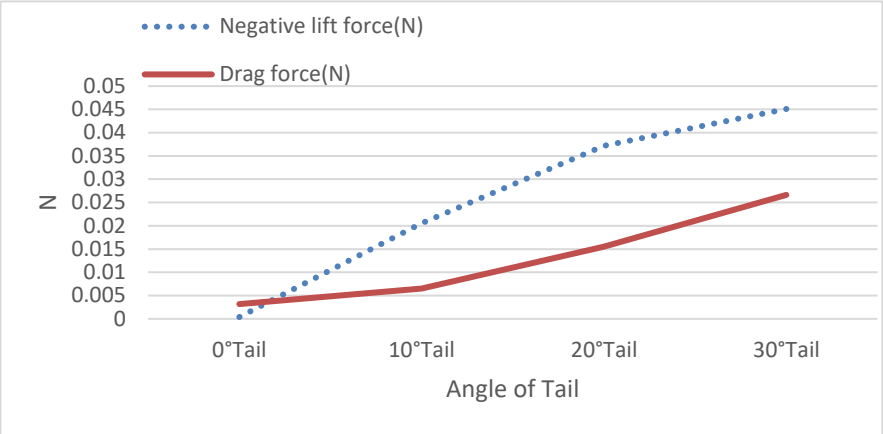

Figure 4.3:Drag, Cd, Negative Lift, Cl under 5m/s inlet velocity

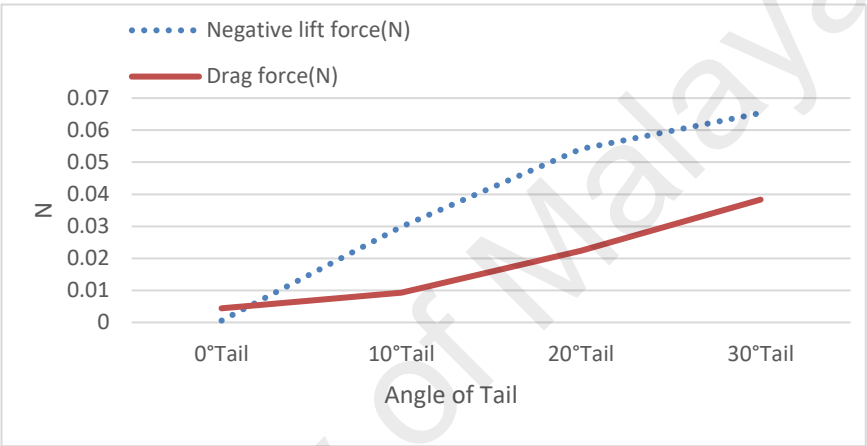

Figure 4.4:Drag, Cd, Negative Lift, Cl under 6m/s inlet velocity

From Figure 4.1 to 4.4, which can deduce that the negative lift force and drag force have an increasing trend with the inlet velocity from 3m/s to 6m/s, but their changing trends are different. As we can see that the slope of the negative lift force after the 20° tail point is getting gradual. Moreover, the slope of the drag force is getting steep after the 10° tail point. In order to obtain a large magnitude of negative lift force and make sure the drag force is reasonable. We need to choose an optimum tail angle, in which the negative lift force with a steep slope and the drag force with a gradual slope. Thus, the relatively reasonable tail angle is 10° and 20° in this project according to the comparison of the above slope. In order to simulate real the flying attitude, we have to consider another important part that is pitch angle. Table 4.5 shows detail of different tail angles with pitch angle from negative 45° to positive 45°.

Table 4.5:Detail of different tail angle and pitch angle

Pitch Angle (°)		Negative lift (N)	Drag (N)	Cd	Cl	Frontal Area
0° Tail	-45	0.0122874	0.013221371	0.5751021	0.534476	0.00417045
	-10	0.007973	0.002795212	0.2556675	0.729263	0.00198331
	-5	0.0040902	0.001714223	0.2109502	0.50334	0.00147414
	0	0.000169	0.001366784	0.2072736	0.025626	0.00119621
	5	-0.003684	0.001606805	0.1316888	-0.30189	0.00221343
	10	-0.00746	0.002590546	0.3000226	-0.82666	0.00156635
	45	-0.012705	0.012962437	0.6062877	-0.51551	0.00387846
10° Tail	-45	0.011019	0.015979257	0.5759748	0.397182	0.00503274
	-10	0.0140043	0.006131145	0.4588902	1.048162	0.00242373
	-5	0.0114302	0.004249152	0.4008097	1.07818	0.00192316
	0	0.0077329	0.002639	0.2713921	0.79524	0.00176398
	5	0.003832	0.001610463	0.2111823	0.502495	0.00138339
	10	-0.0000406	0.00137688	0.0996637	-0.00294	0.00250617
	45	-0.014167	0.010731746	0.5125551	-0.67662	0.00379823
20° Tail	-45	0.0061376	0.01945629	0.6840526	0.215787	0.00515967
	-10	0.013081	0.011143034	0.6299196	0.739471	0.003209
	-5	0.0137625	0.009966637	0.5986123	0.826598	0.00302033
	0	0.0148438	0.00900004	0.6407791	1.056839	0.00254793
	5	0.0147529	0.007471468	0.5320762	1.050622	0.00254732
	10	0.0131258	0.005610618	0.4948412	1.15766	0.00205682
	45	-0.011783	0.004843987	0.3278028	-0.79741	0.00268066

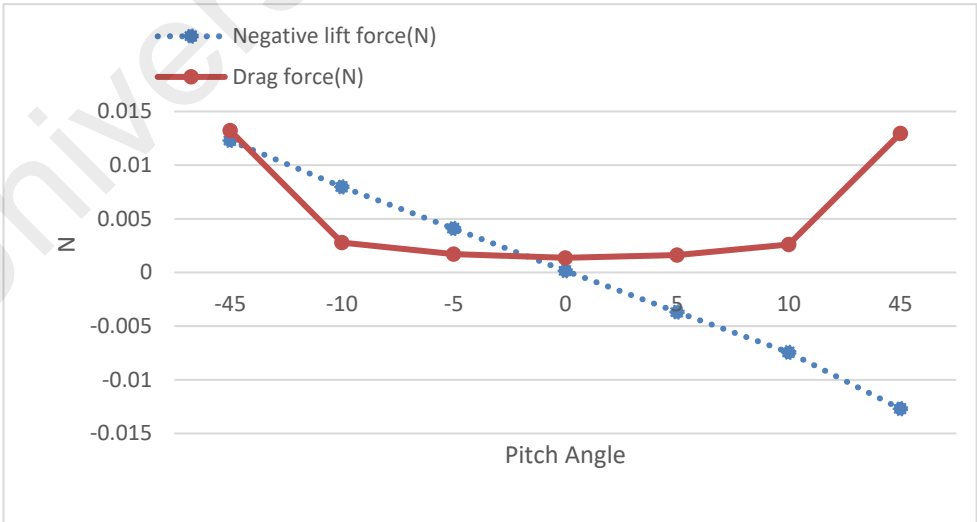

Figure 4.3:Negative lift force and drag force of 0°tail in different pitch angle

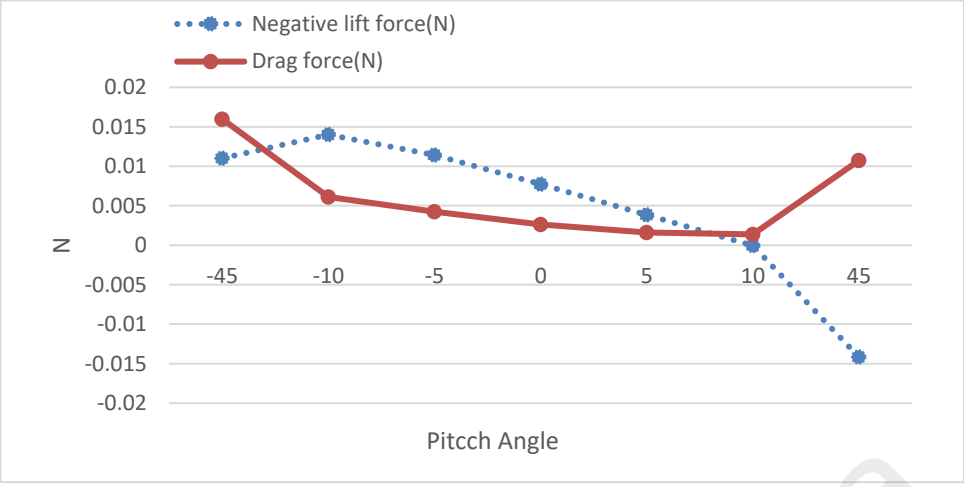

Figure 4.4:Negative lift force and drag force of 10°tail in different pitch angle

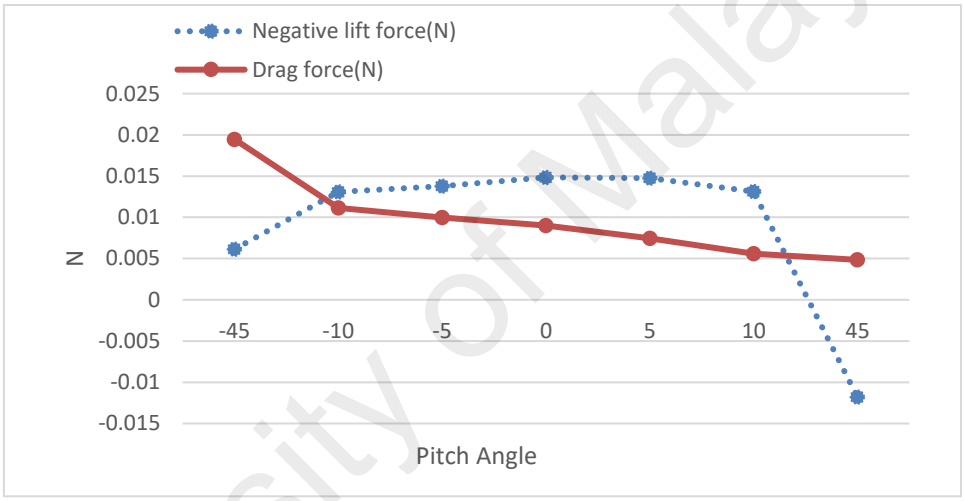

Figure 4.5:Negative lift force and drag force of 20°tail in different pitch angle

In Figure 4.5, the negative lift force is just 0.000169N which is very close to zero negative lift force. The zero negative lift force does not meet the requirement of this project. In Figure 4.6, the negative lift force is -0.000046N at the 10° pitch angle point. But after the 10° pitch angle point, the negative lift becomes positive lift, and the drag will suddenly increase. In Figure 4.7, the negative lift force is 0.0131258N at the 10° pitch angle point, and the drag force is still decreasing. In conclusion, the positive pitch can perform hover flight. The 0° tail angle cannot provide positive pitch angle. The 10° tail angle can only provide 10° pitch angle. The 20° tail angle can provide more than 30° pitch angle.

4.1.2 Velocity

In order to simulate the real flying attitude, some different angles of the body need to be set, which are -45°, -10°, -5°, 0°, 5°, 10°, 45°. Therefore, need to adjust the body in the Virtual Wind Tunnel (computational domain). In the meantime, the inlet velocity should be set in different magnitudes which are 2 m/s, 3m/s, 4m/s, 5m/s, and 6 m/s. In addition, the subject of this research is analysis of body and tail of a flapping drone, the relationship between the body and tail need to be researched. Therefore, the angle of tail 0°, 10°, and 20° are set. The following Figure 4.8 shows the velocity in same pitch angle and different angle of tail. From Figure 4.9 to Figure 4.11 show the velocity in different pitch angle(-45°, -10°, -5°, 0°, 5°, 10°, 45°) and different angle of tail(0°, 10°, 20°).

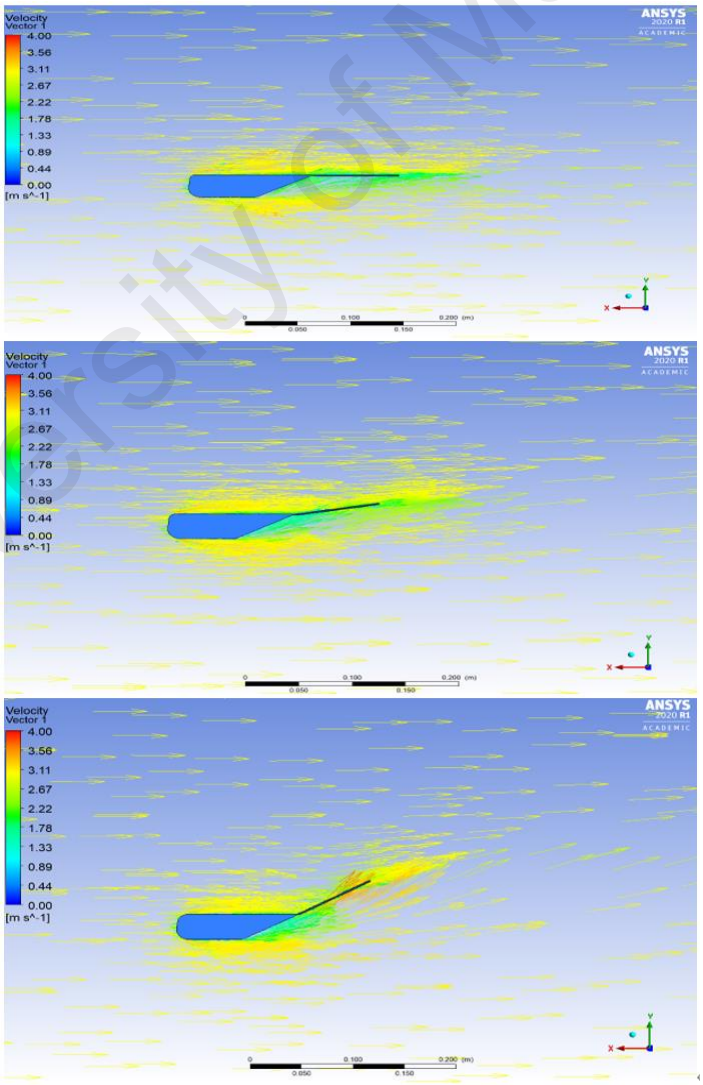

Figure 4.6:0° Pitch angle velocity profile in 0°，10°，20° tail angle

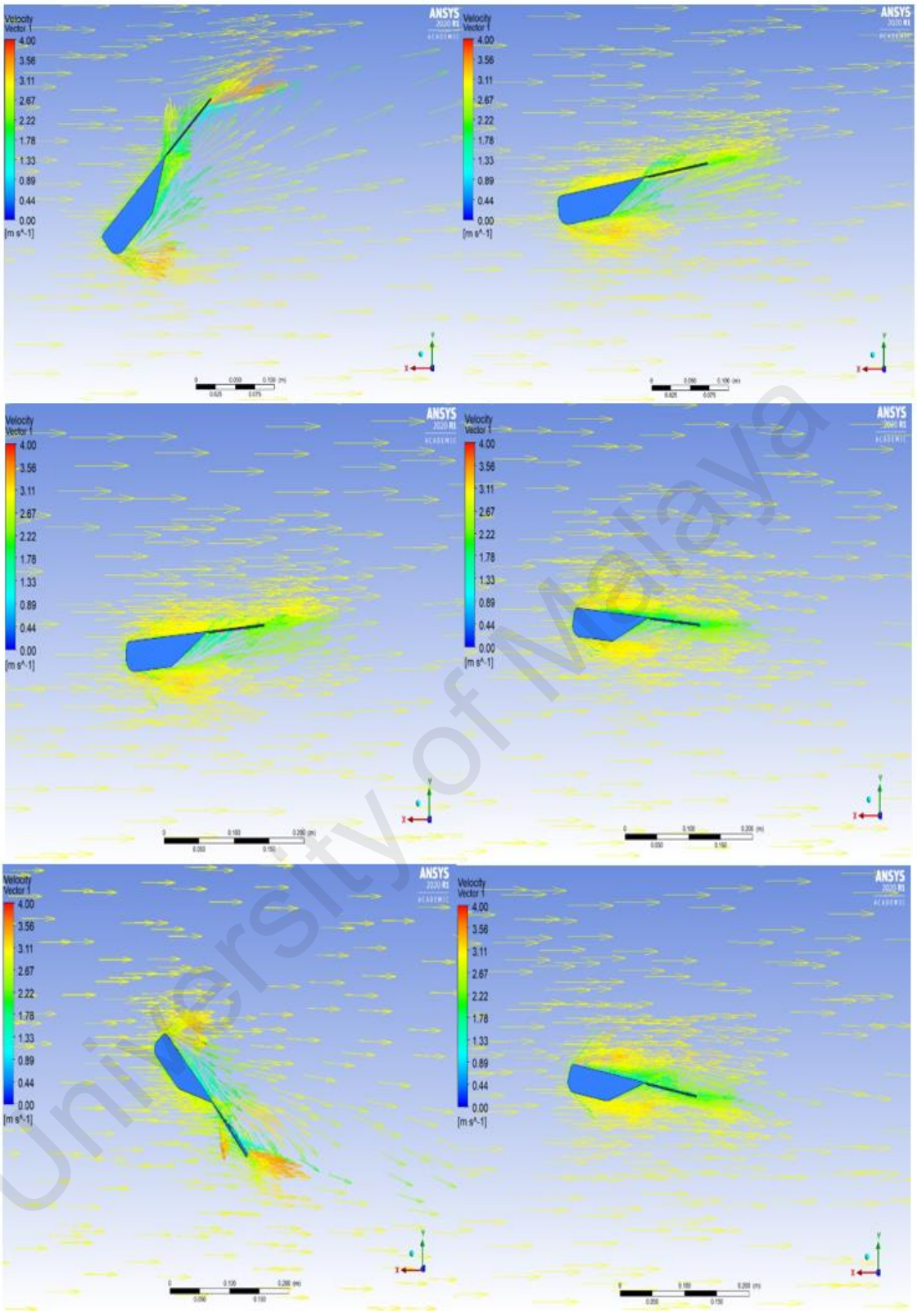

Figure 4.7:0° tail angle under pitch angle from -45° to +45°

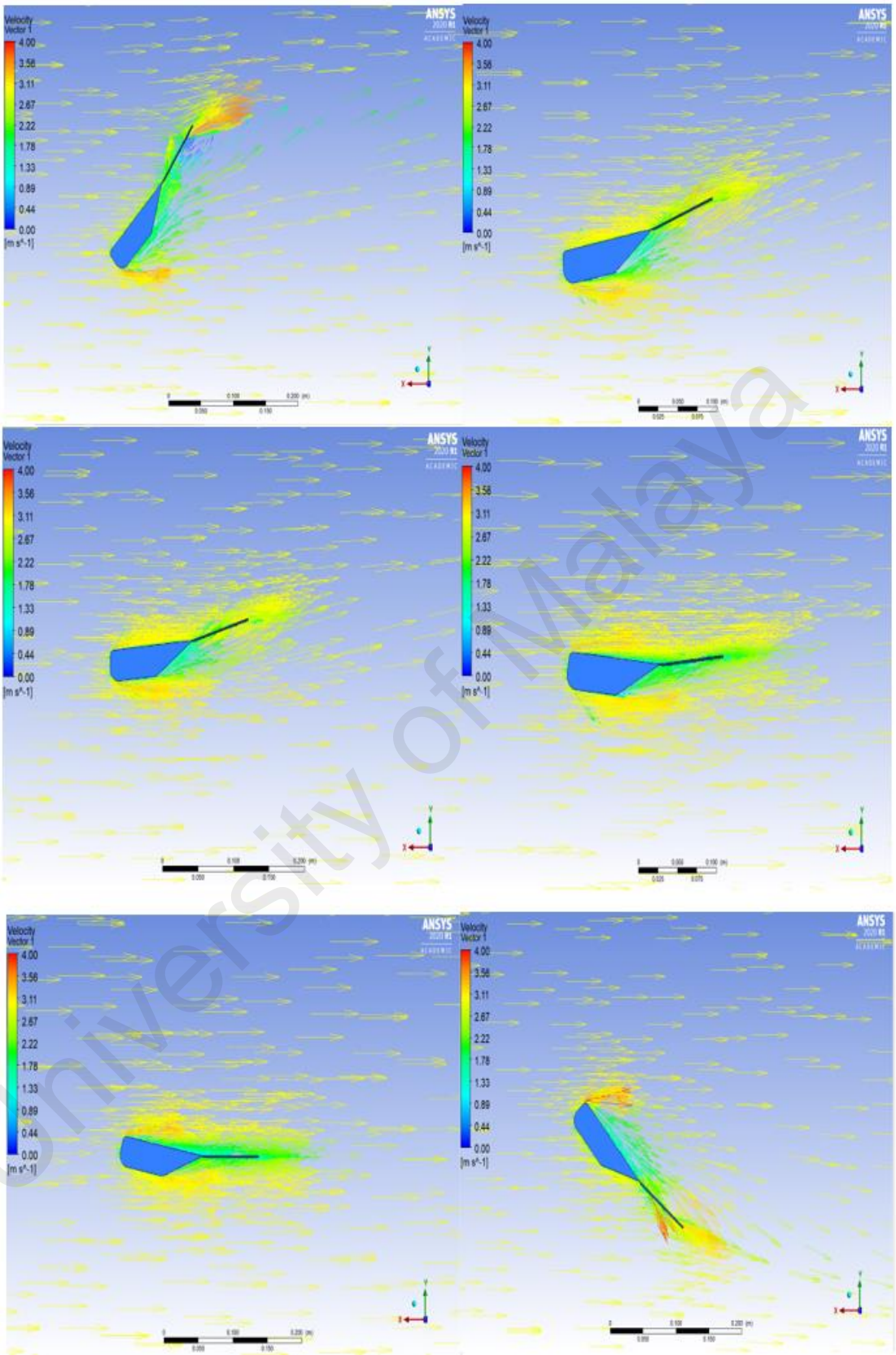

Figure 4.8:10° tail angle under pitch angle from -45° to +45°

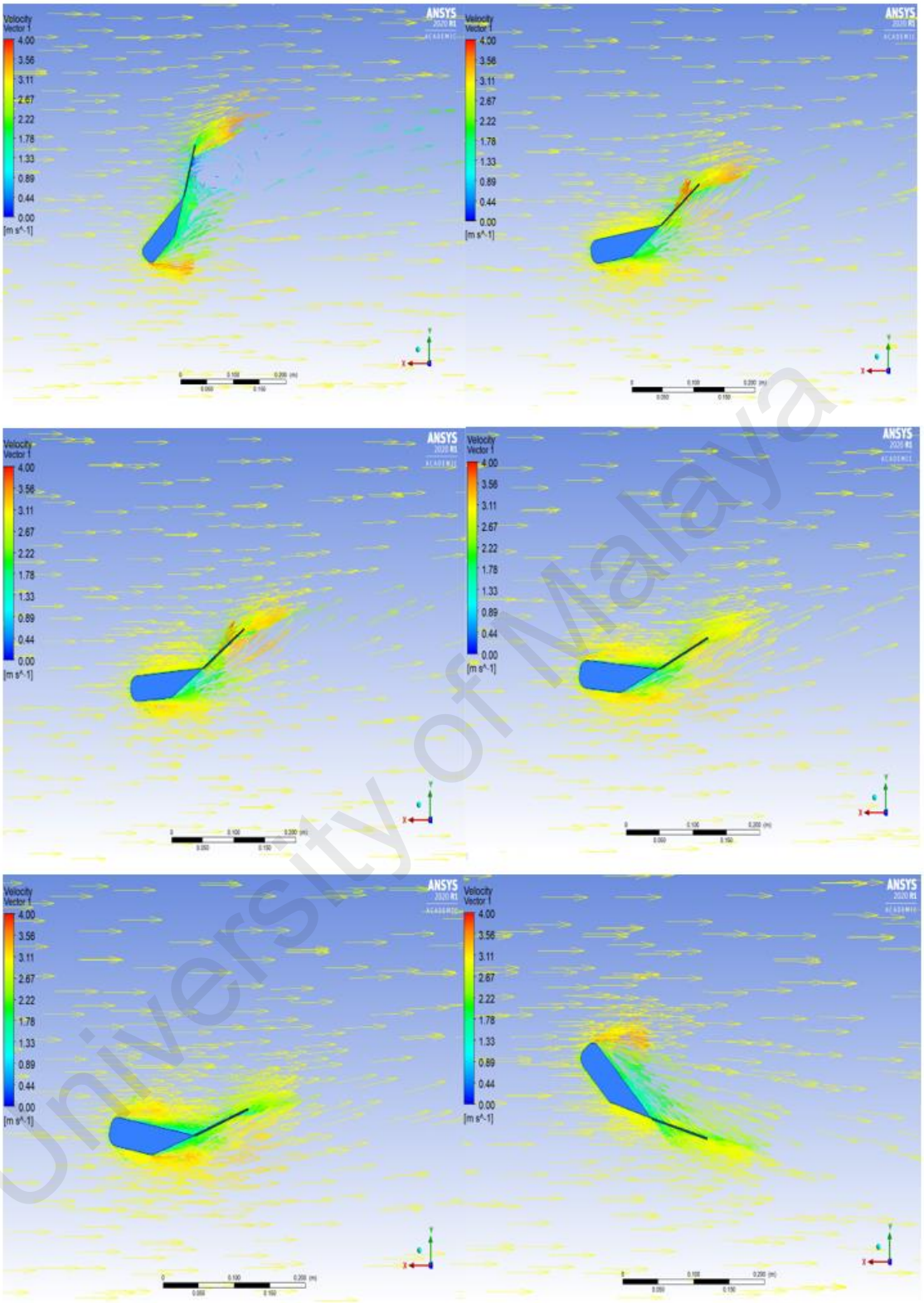

Figure 4.9:20° tail angle under pitch angle from -45° to +45°

4.1.3 Pressure

In order to observe the distribution of pressure on the fuselage more intuitively. From Figure 4.12 to Figure 4.15 show details of pressure distribution. In Figure 4.12, the tail angles are 0°, 10°, and 20°, the pitch angle is 0°. In Figure 4.13, 4.14, and 4.15 the pitch angles are from -45°to +45°respectively, in which the tail angles are 0°, 10°, and 20° respectively.

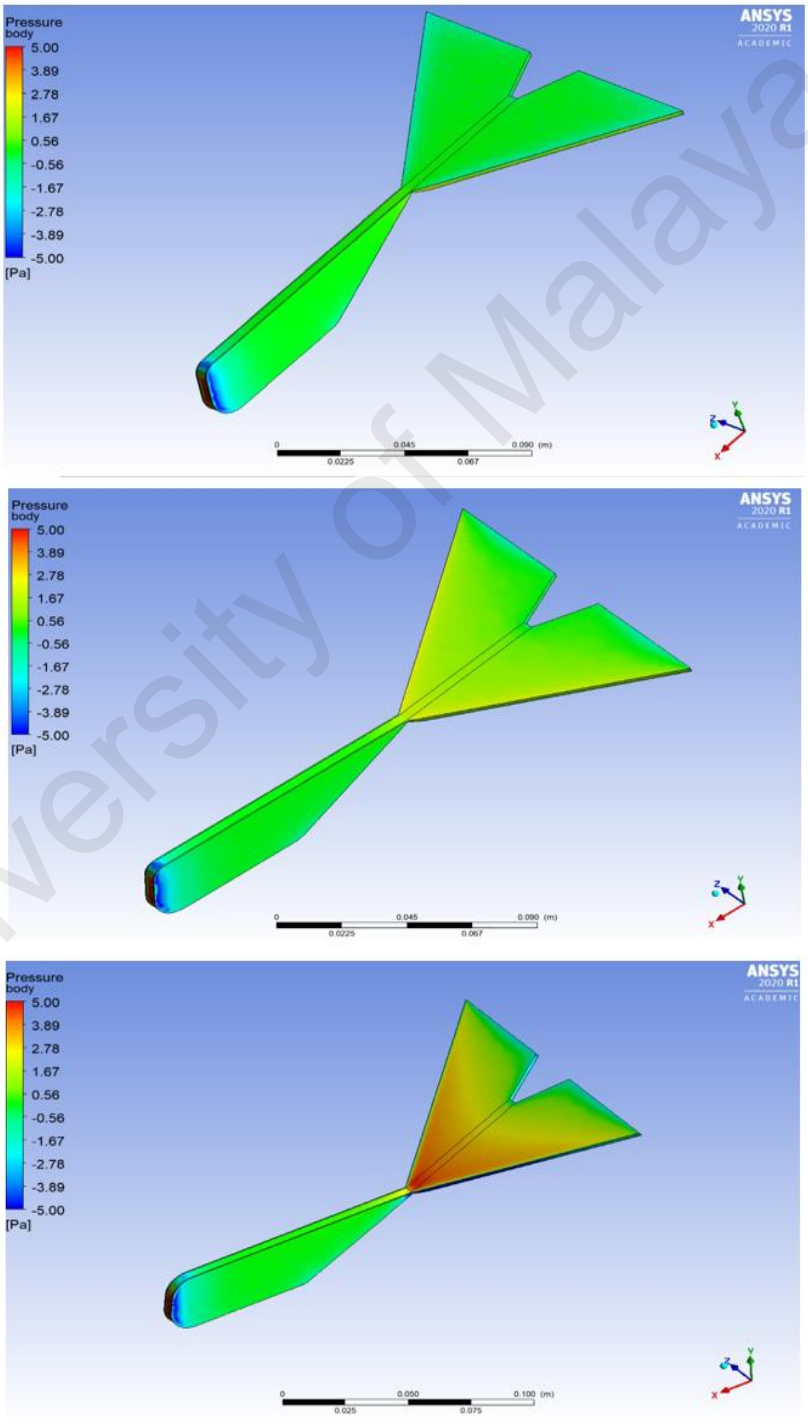

Figure 4.10:0°Pitch angle under the different pressure

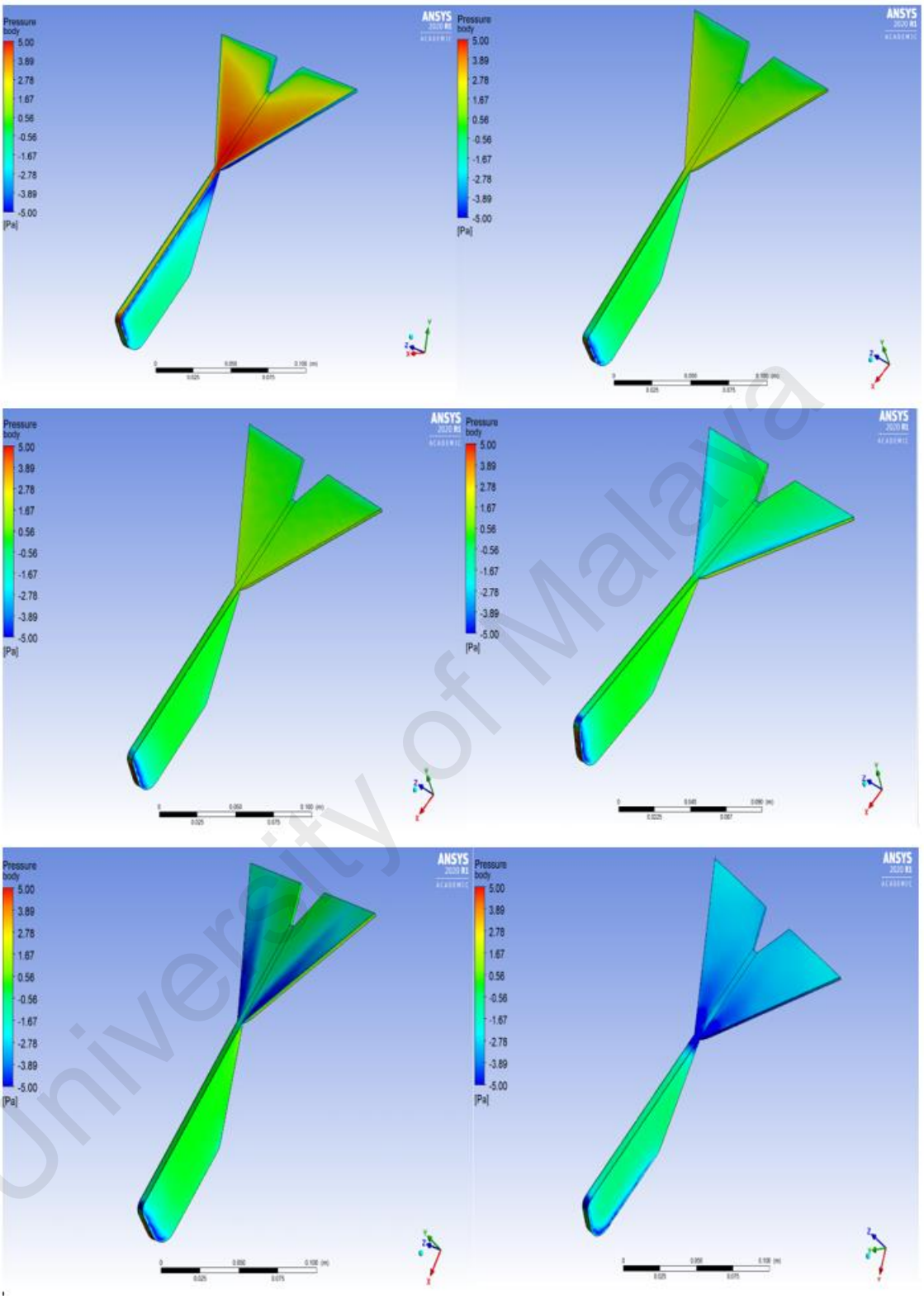

Figure 4.11:0°tail under the different pressure

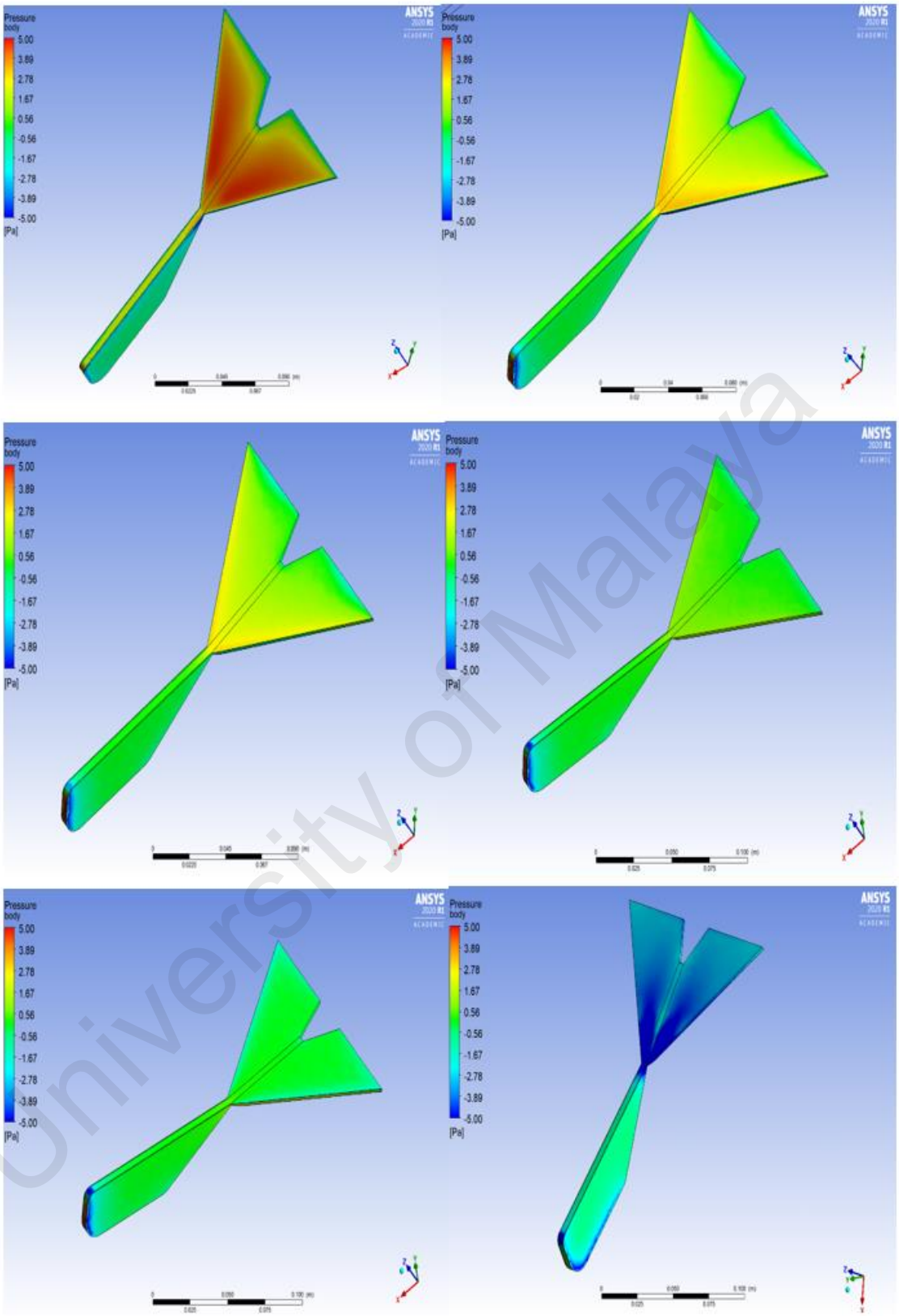

Figure 4.12:10°tail under the different pressure

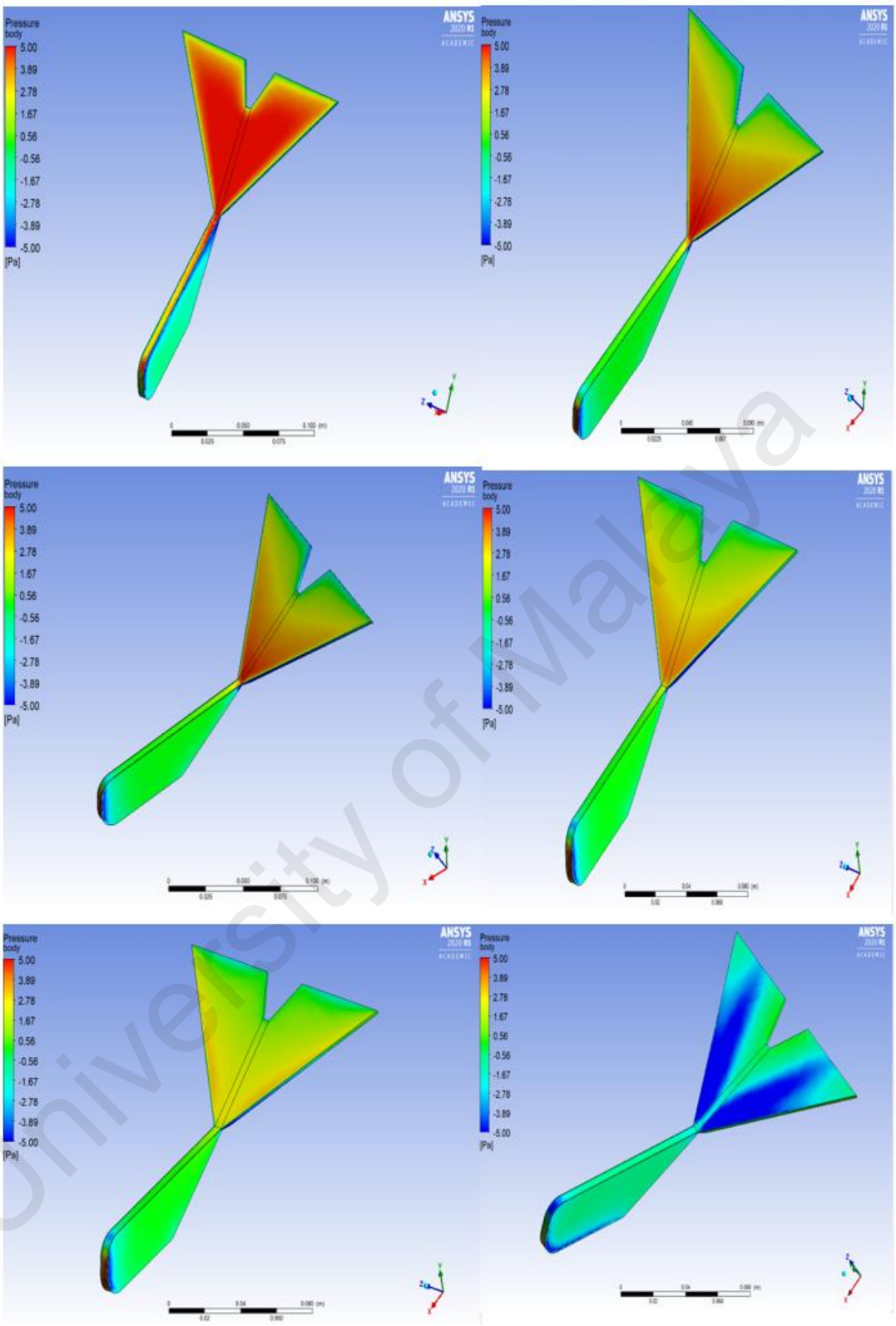

Figure 4.13:20°tail under the different pressure

We can see from Figure 4.10 to 4.13 that under different tail angles and different pitch angles, the pressure distribution on the tail is different. But one thing in common is that all pressure changes start from the front part of the tail where is close to the position of the body.

4.1.4 Connection between CFD finding and actual model

4.1.4.1 Moment of the tail

Like traditional airplanes, the tail of a micro aerial vehicle based on flapping wing is used for trimming, maintaining stability, and gaining maneuverability. During the flight, the tail generates an aerodynamic force. The aerodynamic force generates torque around the center of gravity due to the tail lever arm. Trim means that the torque generated by the tail can make the whole aircraft reach a moment balance.

As an initial mass 30g which is the average mass of the flapping drone were used. This estimation was this project's starting point. Now, the mass of the flapping mechanism, actuator, batteries, receiver, and materials of the components were known. Thus, the better mass estimation and determination of the center of gravity location can be done with these known masses and materials. Figure 4.16 shows the CG location of the flapping drone. Table 4.6 to 4.9 show the moment of the tail in different tail angle under different inlet velocity.

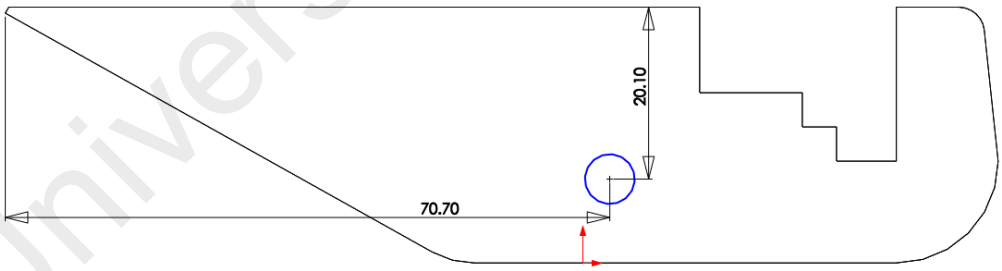

Figure 4.14:CG location

Table 4.6:Inlet velocity 3m/s

Angle	Negative Lift force(N)	Moment
0°Tail	0.000302391	0.0000338
10°Tail	0.014224073	0.001565928
20°Tail	0.025764146	0.002789999
30°Tail	0.03162245	0.00335862

Table 4.7:Inlet velocity 4m/s

Angle	Negative Lift Force(N)	Moment
0°Tail	0.000502055	0.0000561
10°Tail	0.025930874	0.00285473
20°Tail	0.04690465	0.005079305
30°Tail	0.057149136	0.00606981

Table 4.8:Inlet velocity 5m/s

Angle	Negative Lift force(N)	Moment
0°Tail	0.000773833	0.0000864
10°Tail	0.041106874	0.004525456
20°Tail	0.074385582	0.008055215
30°Tail	0.090171256	0.009577089

Table 4.9:Inlet velocity 6m/s

6m/s	Negative Lift force(N)	Moment
0°Tail	0.001132231	0.0001265
10°Tail	0.059684838	0.006570704
20°Tail	0.108225368	0.011719725
30°Tail	0.130656946	0.013877074

Due to the effect of the tail, the aerodynamic center of the whole flapping drone will move behind the center of gravity, so that it can have static stability. The deflection of the tail will generate a control moment. So the flapping drone has the ability to change the flight attitude or maintain balance under different flight attitudes. After comparison the Table 4.6 to 4.9, the moment will change with the change of tail angle and inlet velocity. The large moment may make the fuselage lose its stability, so it needs to be observed and verified in the actual experiment.

4.1.4.2 Velocity measurement

Base on the design of the tail and body, we measured the wind velocity of the tail with a high accuracy velocity meter (Hot Wire Anemometer). Figure 4.17 shows the points that we planned to measure the air velocity. The distance between each point is 30 mm,

and the distance between point 1 and Centre point is 5 mm. The Centre Point is the midpoint of the edge where is the connection between body and tail. For the 0 tail°, the measurement error between simulation value and experimental value is approximately 6.59% on average. For the 20° tail, the measurement error between simulation value and experimental value is approximately 21.14% on average. These measurement errors may cause by the inconsistency of coordinate, equipment.

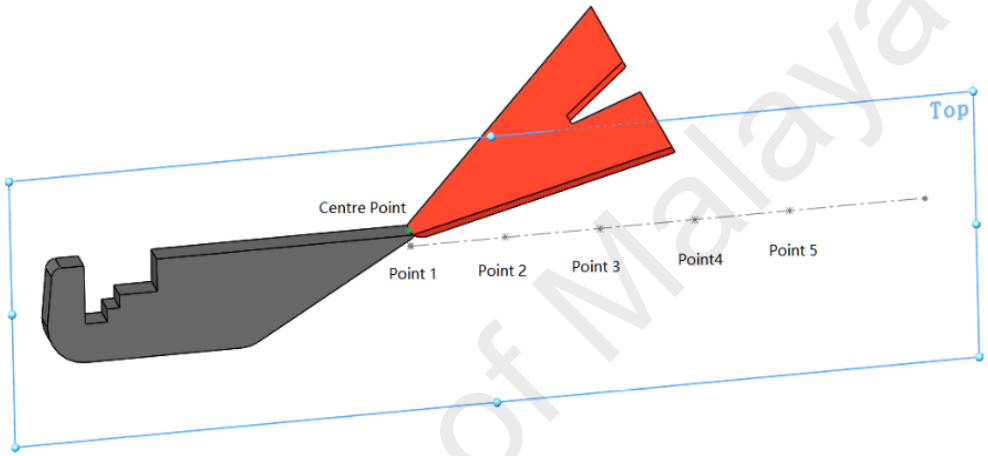

Figure 4.15:The design point for measuring the velocity profile

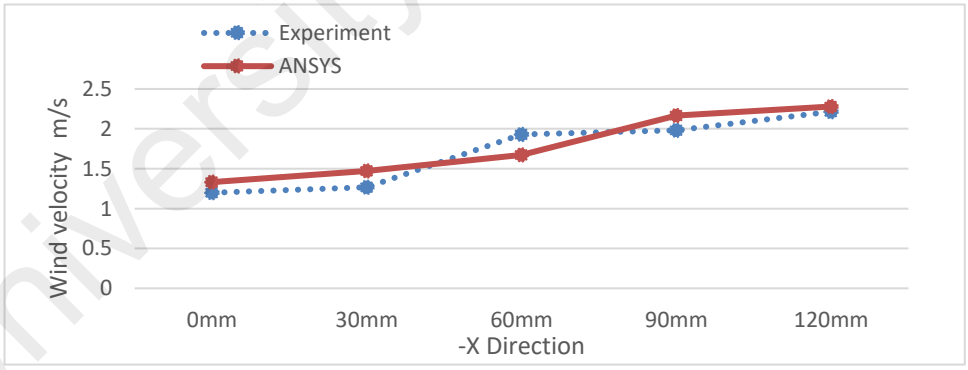

Figure 4.16: ANSYS and actual velocity profile in 0° tail

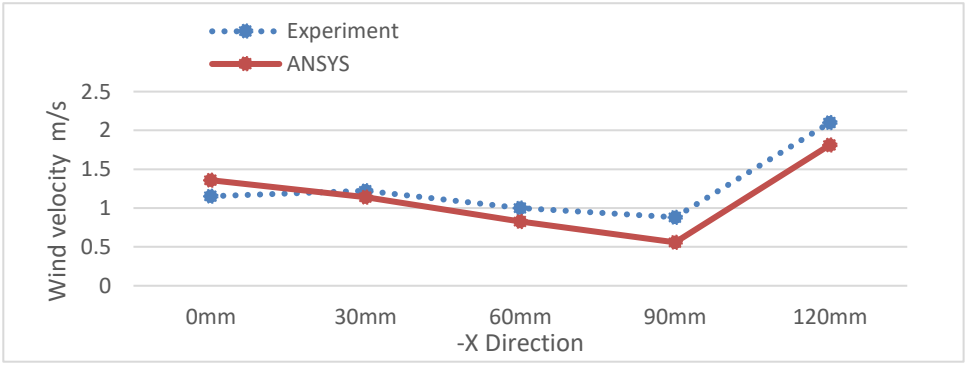

Figure 4.17: ANSYS and actual velocity profile in 20° tail

4.2 Experiment

4.2.1 Actual model

In this experiment, flapping drone with different fuselage shapes and different tail shapes were manufactured. In the final comparison experiment, a model with the same size and the same tail angle as the CFD model was selected for actual testing. Figure 4.20 shows some different shapes and size actual models of flapping drone without assembling wing.

Figure 4.18:Actual models

4.2.2 Testing flight performance

After the actual test, the experimental results corresponded to the CFD simulation results. For the actual test, the flapping drone had a high-speed during the take-off phase. The moment generated by 30° tail caused the fuselage to overturn immediately at the beginning of the take-off stage. This phenomenon verified the instability of the 30° tail at

the start stage. In order to avoid this situation, the head of the fuselage needs to be adjusted with a certain angle. In addition, the power consumption was very fast. The flight time shorter than 0° tail, 10° tail, and 20° tail, this phenomenon resulted from the lager drag force value generated by tail. The normal flight time is around 8 minutes, but through experimental comparison, the flight time of 20° tail was 6 minutes 50 seconds. The flight time of 30° tail was only 5 minutes 20 seconds. For the 0°Tail, due to the "Zero" negative lift force, there was instability of the fuselage during the take-off phase. The head crashed the floor at the beginning of the take-off phase. For the 10° Tail, although the flapping drone did not crash the floor, it cannot fly upward. For the 20°Tail, the flapping drone could perform hover, and more stable than 30°tail. During the flight, the negative lift and landing could be adjusted by controlling the flight speed. In addition, the 10° tail's flight time was 7 minutes and 20 seconds. In short, this test of flight performance was in line with the expectations of CFD simulation. The below Table 4.10 shows details of the flight performance. The Figure 4.21 and 4.22 show actual testing process.

Table 4.10:Performance Testing

Angle of Tail	Duration of Flight	Maximum Flight Altitude	Flight Stability (1-10)
0	-	0m	1
10	456s	1.5m	5
20	411s	4.3m	7
30	319s	6.35m	4

Figure 4.19:Testing 1

Figure 4.20:Testing 2

CHAPTER 5: CONCLUSIONS

Analysis of body and tail of a flapping drone based on CFD simulation and actual experiment was carried out. The different angles (0°, 10°, 20°, 30°) of the tail under the different inlet velocity that from 3m/s to 6m/s as well as different pitch angles (-45°, -10°, -5°, 0°, 5°, 10°, 45°) on the flight performance were investigated. The following listed findings in this research project:

- The lift is getting bigger with the increased speed of the airflow from the inlet surface. Especially in the take-off phase of the flapping drone, a higher initial speed is required to obtain the lift. In this case, the negative lift generated by the tail will also increase. In general, the angle of the tail has a certain range to control the pitch angle to avoid the fuselage "back flip" during the take-off phase. After simulation and experimental tests, the 30°angle of the tail did not meet the design requirements of the model in this study. The reasonable angle of the tail is 20° in this report. This report provided a basis for the tail angle range on the prototype.
- The airflow pressure distribution on the fuselage is different in each pitch angle, especially on the tail. This means the tail plays an important role in the flapping drone. For 0° tail, the negative lift force is just 0.000169N in 0° pitch angle. The 0.000169N is very close to zero negative lift force and does not meet the requirement of this project. For 10° tail, the negative lift force is -0.000046N in 10° pitch angle, but after 10°pitch angle point, the negative lift force becomes positive lift force, and the drag force will suddenly increase. For 20°tail, the negative lift force is 0.0131258N in 10° pitch angle, and the drag force still keeps decreasing. Thus, 20° tail is reasonable for this project. And

the flapping drone in this project cannot perform a negative pitch angle, the only way to land is to decrease the frequency of the flapping wing.

5.1 FUTURE WORKS

- Due to the time constraints and the complexity of the flapping drone movement, the model of the wing part was not included when considering the angle relationship between the tail and the fuselage. The flapping wing mechanism should be considered in future studies.
- In order to enable flapping drone to obtain better maneuverability, in future research, an additional rudder can be added on the tail to control the whole surface of the tail to realize two degrees of freedom.
- Due to the lack of relative measuring equipment, the actual experiment did not include the measurement of the lift and cl. In the future works, we need to measure the actual lift and drag of the flapping drone and compare with the simulation results.

REFERENCES

Abas, M. F. B., Rafie, A. S. B. M., Yusoff, H. B., & Ahmad, K. A. B. J. C. J. o. A. (2016). Flapping wing micro-aerial-vehicle: kinematics, membranes, and flapping mechanisms of ornithopter and insect flight. *29*(5), 1159-1177.

Alfonsi, G. J. A. M. R. (2009). Reynolds-averaged Navier–Stokes equations for turbulence modeling. *62*(4).

Altinisik, A., Kutukceken, E., & Umur, H. J. J. o. F. E. (2015). Experimental and numerical aerodynamic analysis of a passenger car: Influence of the blockage ratio on drag coefficient. *137*(8).

Anderson, M. L. (2011). *Design and control of flapping wing micro air vehicles*. Retrieved from

Armanini, S., Caetano, J., De Visser, C., Pavel, M., De Croon, G., & Mulder, M. J. I. J. o. M. A. V. (2019). Modelling wing wake and tail aerodynamics of a flapping-wing micro aerial vehicle. *11*, 1756829319833674.

Atmaca, M., Çetin, B., & Yılmaz, E. J. A. P. P. A. (2019). CFD analysis of unmanned aerial vehicles (UAV) moving in flocks. *135*(4), 694-696.

Biswal, S. (2015). *Modeling and control of flapping wing micro aerial vehicles*: Arizona State University.

Çengel, Y. A., & Cimbala, J. M. (1996). Introduction to Computational Fluid Dynamics.

De Croon, G., De Clercq, K., Ruijsink, R., Remes, B., & De Wagter, C. J. I. J. o. M. A. V. (2009). Design, aerodynamics, and vision-based control of the DelFly. *1*(2), 71-97.

Delfly Ⅰ. Retrieved from http://www.delfly.nl/micro/

Fenelon, M. A., Furukawa, T. J. M., & Theory, M. (2010). Design of an active flapping wing mechanism and a micro aerial vehicle using a rotary actuator. *45*(2), 137-146.

Gerdes, J. W. (2010). *Design, Analysis, and testing of a flapping wing miniature air vehicle.*

Hall, K. C., & Hall, S. R. J. J. o. F. M. (1996). Minimum induced power requirements for flapping flight. *323*, 285-315.

Harputlu, Ö. (2014). *Numerical and experimental analysis of a piezoelectric flat plate in flapping motion.* MIDDLE EAST TECHNICAL UNIVERSITY,

Ho, S., Nassef, H., Pornsinsirirak, N., Tai, Y.-C., & Ho, C.-M. J. P. i. A. S. (2003). Unsteady aerodynamics and flow control for flapping wing flyers. *39*(8), 635-681.

Junkui, C. (2015). *Numerical Simulation for Aerodynamic Characteristics of Asymmetric"Diamond back" Wing at Low Reynolds Number.* North University of China

Lankford, J. (2018). *Experimental and coupled CFD/CSD investigation of flexible MAV-scale flapping wings in hover*.

Lee, Y., Lua, K. B., Lu, H., Aisyah, S., & Lim, T. (2016). *Aerodynamics of 2D and 3D flapping wings in water treading motion.* Paper presented at the Proceedings of 20th Australasian fluid mechanics conference.

Leonardo da Vinci's ornithopter design. Retrieved from https://en.wikipedia.org/wiki/Ornithopter

Maglasang, J., Isogai, K., Goto, N., & Yamasaki, M. J. M. o. t. F. o. E., Kyushu University. (2006). Aerodynamic study and mechanization concepts for flapping-wing micro aerial vehicles. *66*(1), 71-82.

McMichael, J. M. J. h. w. a. g. t. M. m. a. h. (1997). Micro air vehicles-toward a new dimension in flight.

Michelson, R. C., & Reece, S. (1998). *Update on flapping wing micro air vehicle research-ongoing work to develop a flapping wing, crawling entomopter.* Paper presented at the 13th Bristol International RPV/UAV Systems Conference Proceedings, Bristol England.

Mystkowski, A., & Jastrzębski, R. J. J. o. V. (2013). Vibrating a small plate vortex generator to improve control robustness of a micro aerial delta wing vehicle. *15*(1), 114-123.

Nabawy, M., ElNomrossy, M., Abdelrahman, M., & ElBayoumi, G. J. T. A. J. (2012). Aerodynamic shape optimisation, wind tunnel measurements and CFD analysis of a MAV wing. *116*(1181), 685-708.

Nedunchezian, K., Kang, C.-k., Aono, H. J. J. o. S., & Vibration. (2019). Effects of flapping wing kinematics on the aeroacoustics of hovering flight. *442*, 366-383.

Orlowski, C., Girard, A., & Shyy, W. (2010). *Open loop pitch control of a flapping wing micro-air vehicle using a tail and control mass.* Paper presented at the Proceedings of the 2010 American Control Conference.

Orlowski, C. T., & Girard, A. R. J. P. i. A. S. (2012). Dynamics, stability, and control analyses of flapping wing micro-air vehicles. *51*, 18-30.

Pornsin-Sirirak, T. N., Tai, Y.-C., Ho, C.-M., & Keennon, M. (2001). *Microbat: A palm-sized electrically powered ornithopter.* Paper presented at the Proceedings of NASA/JPL Workshop on Biomorphic Robotics.

Rozhdestvensky, K. V., & Ryzhov, V. A. J. P. i. a. s. (2003). Aerohydrodynamics of flapping-wing propulsors. *39*(8), 585-633.

Sahini, D. (2004). *Wind tunnel blockage corrections: a computational study*. Texas Tech University,

Send, W., Fischer, M., Jebens, K., Mugrauer, R., Nagarathinam, A., & Scharstein, F. (2012). *Artificial hinged-wing bird with active torsion and partially linear kinematics.* Paper presented at the Proceeding of 28th Congress of the International Council of the Aeronautical Sciences.

Shyy, W., Aono, H., Chimakurthi, S. K., Trizila, P., Kang, C.-K., Cesnik, C. E., & Liu, H. J. P. i. A. S. (2010). Recent progress in flapping wing aerodynamics and aeroelasticity. *46*(7), 284-327.

Shyy, W., Lian, Y., Tang, J., Liu, H., Trizila, P., Stanford, B., . . . Ifju, P. J. A. M. S. (2008). Computational aerodynamics of low Reynolds number plunging, pitching and flexible wings for MAV applications. *24*(4), 351-373.

Smart Bird by Festo company. Retrieved from https://www.festo.com/group/en/cms/10238.htm

Trizila, P., Kang, C.-K., Aono, H., Shyy, W., & Visbal, M. J. A. j. (2011). Low-Reynolds-number aerodynamics of a flapping rigid flat plate. *49*(4), 806-823.

Tsai, B.-J., Fu, Y.-C. J. A. S., & Technology. (2009). Design and aerodynamic analysis of a flapping-wing micro aerial vehicle. *13*(7), 383-392.

Yang, Y., & Li, L. (2012). *Influence of flapping wing unsteady motion on aerodynamic performance of horizontal tail.* Paper presented at the 28th International Congress of the Aeronautical Sciences, Brisbane, Australia.

Zhang, P., Zhu, J., & Zhu, Y. J. J. o. R. (2020). Analysis on Hover Control Performance of T-and Cross-Shaped Tail Fin of X-Wing Single-Bar Biplane Flapping Wing. *2020*.

Zhang, Z., Li, J., Li, T., & WANG, J.-j. J. J. o. E. i. F. M. (2010). Experimental investigation of split-rudder deflection on aerodynamic performance of tailless flying-wing aircraft. *24*(3), 63-66.